RQT
.16

EXCIMER LASERS

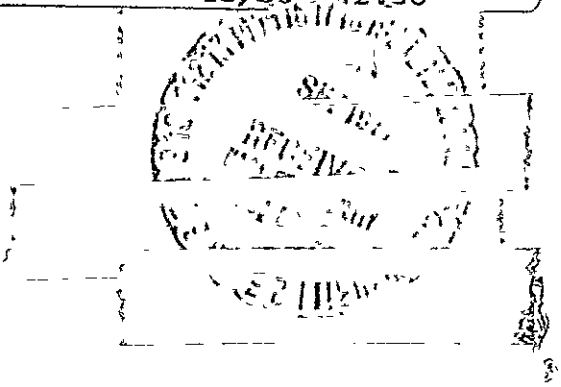

A.J. Palmer, L.D. Hess, and R.R. Stephens

Hughes Research Laboratories
3011 Malibu Canyon Road
Malibu, CA 90265

July 1976

Contract NAS 3--19707
Annual Report 1
For Period 30 May 1975 Through 10 June 1976

Sponsored By
NATIONAL AERONAUTICS AND SPACE ADMINISTRATION
Lewis Research Center
Cleveland, OH

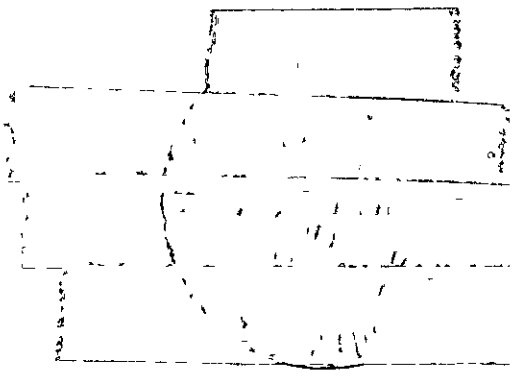

UNCLASSIFIED

SECURITY CLASSIFICATION OF THIS PAGE *(When Data Entered)*

REPORT DOCUMENTATION PAGE		READ INSTRUCTIONS BEFORE COMPLETING FORM
1 REPORT NUMBER	2 GOVT ACCESSION NO	3 RECIPIENT'S CATALOG NUMBER
4 TITLE *(and Subtitle)* EXCIMER LASERS		5 TYPE OF REPORT & PERIOD COVERED Annual Tech. Rpt. 1 30 May 1975-11 June 1976
		6 PERFORMING ORG REPORT NUMBER
7 AUTHOR(s) A.J. Palmer, L.D. Hess, and R.R. Stephens		8 CONTRACT OR GRANT NUMBER(s) NAS 3-19707
9 PERFORMING ORGANIZATION NAME AND ADDRESS Hughes Research Laboratories 3011 Malibu Canyon Road Malibu, CA 90265		10 PROGRAM ELEMENT PROJECT TASK AREA & WORK UNIT NUMBERS
11 CONTROLLING OFFICE NAME AND ADDRESS National Aeronautics & Space Administration Lewis Research Center Cleveland, Ohio		12 REPORT DATE July 1976 13 NUMBER OF PAGES 95
14 MONITORING AGENCY NAME & ADDRESS *(if different from Controlling Office)*		15 SECURITY CLASS *(of this report)* Unclassified 15a DECLASSIFICATION DOWNGRADING SCHEDULE

16 DISTRIBUTION STATEMENT *(of this Report)*

17 DISTRIBUTION STATEMENT *(of the abstract entered in Block 20, if different from Report)*

18 SUPPLEMENTARY NOTES

19 KEY WORDS *(Continue on reverse side if necessary and identify by block number)*
CW Excimer Lasers
Capillary Discharge Excimer Lasers
XeF, KXe, and K_2 Excimer Molecules

20 ABSTRACT *(Continue on reverse side if necessary and identify by block number)*

A theoretical and experimental investigation into the possibility of achieving cw discharge pumped excimer laser oscillation is reported. An initial literature search identified four candidate cw excimer transitions: the XeF $^2\Sigma_{1/2} \rightarrow {}^2\Sigma_{1/2}$ transition at ~3450 Å; the KXe $^2\pi_{1/2} \rightarrow {}^2\Sigma_{1/2}$ transition at ~8500 Å; the K_2 $^1\Sigma_u^+ \rightarrow {}^1\Sigma_g^+$ transition at ~10400 Å; and the Hg_2 $A\,^3\Sigma_u \rightarrow X\,^1\Sigma_g^+$ transition at 3350 Å. Capillary discharge pumping was identified as an expedient technique by which to gather

DD FORM 1 JAN 73 1473 EDITION OF 1 NOV 65 IS OBSOLETE

UNCLASSIFIED

SECURITY CLASSIFICATION OF THIS PAGE *(When Data Entered)*

basic data and demonstrate laser oscillation for cw operation of these systems. Detailed theoretical modeling of capillary discharge pumping of the XeF and KXe and K_2 excimer systems was carried out which predicted the required discharge parameters for reaching laser threshold on these systems. Capillary discharge pumping of the XeF excimer system was investigated experimentally. The experiments revealed a lower excimer level population density than predicted theoretically by about an order of magnitude. The experiments also revealed a fluorine consumption problem in the discharge in agreement with theory. Attempts to operate the discharge at the elevated pressures required for overcoming the consumption problem are as yet unsuccessful. Experimental apparatus for obtaining data on the capillary discharge pumped KXe and K_2 systems was fabricated according to the theoretically predicted operating requirements. Operation of the discharge tube was delayed and is being continued into the next contract period. Finally, the information gained in this investigation of capillary discharge pumping of the XeF excimer system was used to identify a novel dimensionally scalable cw pumping technique which can be applied to this system for meeting NASA's ultimate output power objectives.

TABLE OF CONTENTS

SECTION		PAGE
	LIST OF ILLUSTRATIONS	5
I	INTRODUCTION	7
II	PRELIMINARY EVALUATION	9
	A Selection of Candidate Excimer Molecules	9
	B. Selection of a CW Pumping Technique	20
III	THEORETICAL EVALUATION	25
	A. Modeling Procedures	25
	B. Results and Discussion	34
IV	LABORATORY APPARATUS	45
V	EXPERIMENTAL RESULTS	53
	A. Introduction	53
	B. Experiments with Tube 1	54
VI	PRELIMINARY CONCLUSIONS AND FUTURE WORK PLAN	79
	A. Preliminary Conclusions	79
	B. Future Work Plan	80
	REFERENCES	85
	APPENDIX	87

LIST OF ILLUSTRATIONS

FIGURE		PAGE
II-1	Excimer and dimer potential energy curves	10
II-2	Evaluation procedure applied to the periodic table	12
II-3	Group 1 — hydrogen	13
II-4	Group 1 — alkali metals: Na, K, Rb, Cs	15
II-5	Transition element subgroup: Zn, Cd, Hg	17
II-6	Groups V and VI — N, P, As, O, S, Se	18
II-7	Group VII — F, Bl, Cl, I	19
II-8	Group VIII — He, Ne, Ar, Kr, Xe	20
II-9	Laser transition data: KXe, K_2	21
II-10	Laser transition data: Hg_2	22
II-11	Laser transition data: XeF	22
III-1	Capillary discharge pumped XeF excimer results: theory versus experiment	39
III-2	Theoretical modeling results for avalanche sustained discharge pumping of the K-Xe/K_2 system	42
III-3	Capillary K_2 pumping: low pressure case	43
IV-1	Rare-gas halide capillary discharge laser apparatus	46
IV-2	Schematic diagram of XeF capillary discharge tube and pulse circuit	46

FIGURE		PAGE
IV-3	Schematic diagram of potassium rare gas discharge apparatus	48
IV-4	Photograph of potassium rare gas apparatus in final stages of fabrication	49
IV-5	Experimental arrangement for absolute fluorescence measurements	50
IV-6	Spectral profile of XeF excimer fluorescence from capillary discharge tube	51
V-1	Quasi-cw operation of a typical NF_3 mixture in the 3 mm tube	56
V-2	Optimized fluorescence for 3 mm tube experiments	58
V-3	Quasi-cw operation in typical NF_3 mixture	61
V-4	Quasi-cw operation in typical F_2 mixture	63
V-5	Operation at 200 Torr with high helium concentration	67
V-6	V-I data for NF_3 mixtures illustrating current density limit	69
V-7	V-I data for NF_3 mixture illustrating the discharge stability condition	72
V-8	Pressure dependence of fluorescence from a typical NF_3 mixture	74
V-9	Optimized fluorescence in 1 mm bore tube for several NF_3 mixtures	76
VI-1	Projected capillary discharge configuration for cw excimer laser	80
VI-2	Low pressure XeF excimer plasma jet concept	80

I. INTRODUCTION

This report covers the first year's work on the NASA/LERC research program on electrically pumped continuous wave (cw) excimer lasers. An excimer laser transition is a transition between two electronic states of a diatomic molecule, the upper state being a bound state and the lower state being an unbound state. Such a transition will exhibit several advantageous features when compared with other types of lasers. These include

- Broad band tunability ($\Delta\lambda$ ~1000 to 2000 Å)
- High cw saturation power (~50 kW/cm^2)
- Large high power system capability (low gain, fewer parasitic problems).

The excimer laser transition is uniquely suited to meeting NASA's ultimate cw high power laser mission requirements.

The primary objectives of the NASA program covered by this report are (1) to identify potential excimer molecules for visible and near visible cw laser operation based on electrical excitation, (2) to predict the specific operating conditions required for such laser action, and (3) to demonstrate cw laser gain on such a system in a laboratory experiment.

To accomplish these objectives, the program was divided into four major tasks:

Task I — Preliminary evaluation
Task II — Analytic evaluation
Task III — Laboratory apparatus
Task IV — Molecular system evaluation.

Specific objectives, procedures, and results for these four tasks will be presented in Sections II through V. Section VI presents preliminary conclusions and the work planned for the next year's follow-on phase of the program.

II PRELIMINARY EVALUATION

The objective of this task is to identify at least three molecular excimer systems suitable for visible or near visible cw laser operation when excited by either a self-sustained or an electron beam-sustained discharge.

Our procedure in addressing this task was to first select the three candidate molecules and to then select a cw electrical pumping technique appropriate for an experimental evaluation of two of the excimer systems under cw conditions.

A. Selection of Candidate Excimer Molecules

Consider again the basic definition of an excimer laser transition as a transition that occurs between two electronic states of a diatomic molecule of which the lower state is a dissociative or repulsive state as in Figure II-1(a). In our selection of candidate cw excimer systems we broaden the definition of an excimer system to include any molecular electronic transition that exhibits a continuum red shift relative to the transition between the associated parent atomic states, since it is this feature that is fundamentally responsible for the ability to maintain a cw population inversion on a broadened molecular electronic transition. To see this, one assumes that the molecular states are populated in thermal equilibrium with respect to their parent atomic states in accordance with the gas temperature, while the population of the atomic states are in thermal equilibrium at the electron temperature. The population ratio between the upper and lower molecular levels then can be written

$$\frac{N_u}{N_\ell} = \exp\left(\frac{\Delta(h\nu)}{T_g} - \frac{h\nu_o}{T_e}\right), \qquad (1)$$

where $\Delta(h\nu)$ is the red shift, $h\nu_o$ is the atomic transition energy, and T_g and T_e is the gas temperature and electron temperature, respectively; we have omitted degeneracy factors for simplicity. Therefore,

an inversion will maintain, under this two-temperature equilibrium condition, if the ratio of gas to electron temperature is less than the fractional red shift, i.e.,

$$\frac{T_g}{T_e} < \frac{\Delta h\nu}{h\nu_o} \quad , \tag{2}$$

regardless of the bound or unbound nature of the molecular potential energy curves. An example situation, which exhibits the required red shift but does not involve a repulsive lower molecular level, is the dimer transition, illustrated in Figure II-1(b), where the red shift is a result of the shift in the internuclear separations of the potential minima of two bound molecular states.

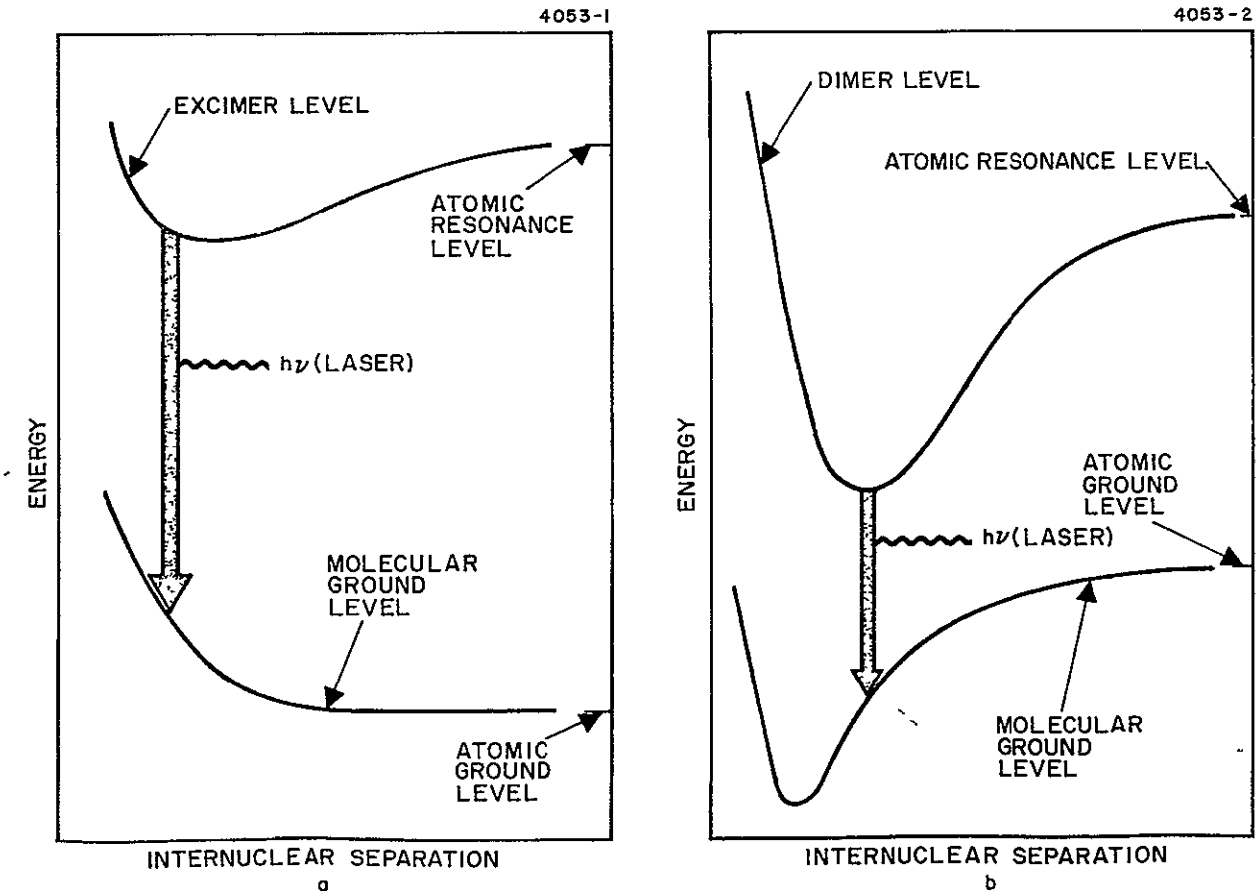

Figure II-1. Excimer and dimer potential energy curves. (a) Excimer. (b) Dimer.

The two-temperature equilibrium condition is a sufficient but not a necessary condition for achieving laser gain on red shifted excimer and dimer transitions. For example, excimer and dimer laser action demonstrated on the vacuum ultraviolet rare-gas excimer and the H_2 dimer transition, respectively, does not occur under two-temperature equilibrium conditions. It is still the red shift, however, that is primarily associated with the ability to achieve a population inversion in these cases.

The search for potential excimer molecules began with the observation that every element in the periodic table will probably form at least one excimer or excimer-like (in the sense defined above) laser transition either in a homonuclear or heteronuclear diatomic molecule. Thus, our preliminary evaluation of potential excimer molecules first involved various processes of elimination applied to the elements of the periodic table (Figure II-2).

The first criterion applied in the elimination procedure is somewhat arbitrary but motivated by the desire for expediency. Since electrical excitation is to be used, it is required that the active medium be in the gas phase. In particular, we consider only those elements which have a vapor pressure greater than one Torr at temperatures below 500°C, and are reasonably abundant and nonradioactive. This leaves us with the following elements (see Figure II-2):

Group I	H, Na, K, Rb, Cs
Group II	None
Transition Elements	Zn, Cd, Hg
Group III	None
Group IV	None
Group V	N, P, As
Group VI	O, S, Se
Group VII	F, Cl, Br, I
Group VIII	He, Ne, A, Kr, Xe

A further narrowing down of the group of candidate excimer systems was then achieved through qualitative considerations on the nature of the known excimer or excimer-like transitions on both the heternuclear

FIRST REQUIREMENTS·

1. VAPOR PRESSURE > 1 Torr AT T < 500 °C
2. REASONABLY ABUNDANT AND NONRADIOACTIVE

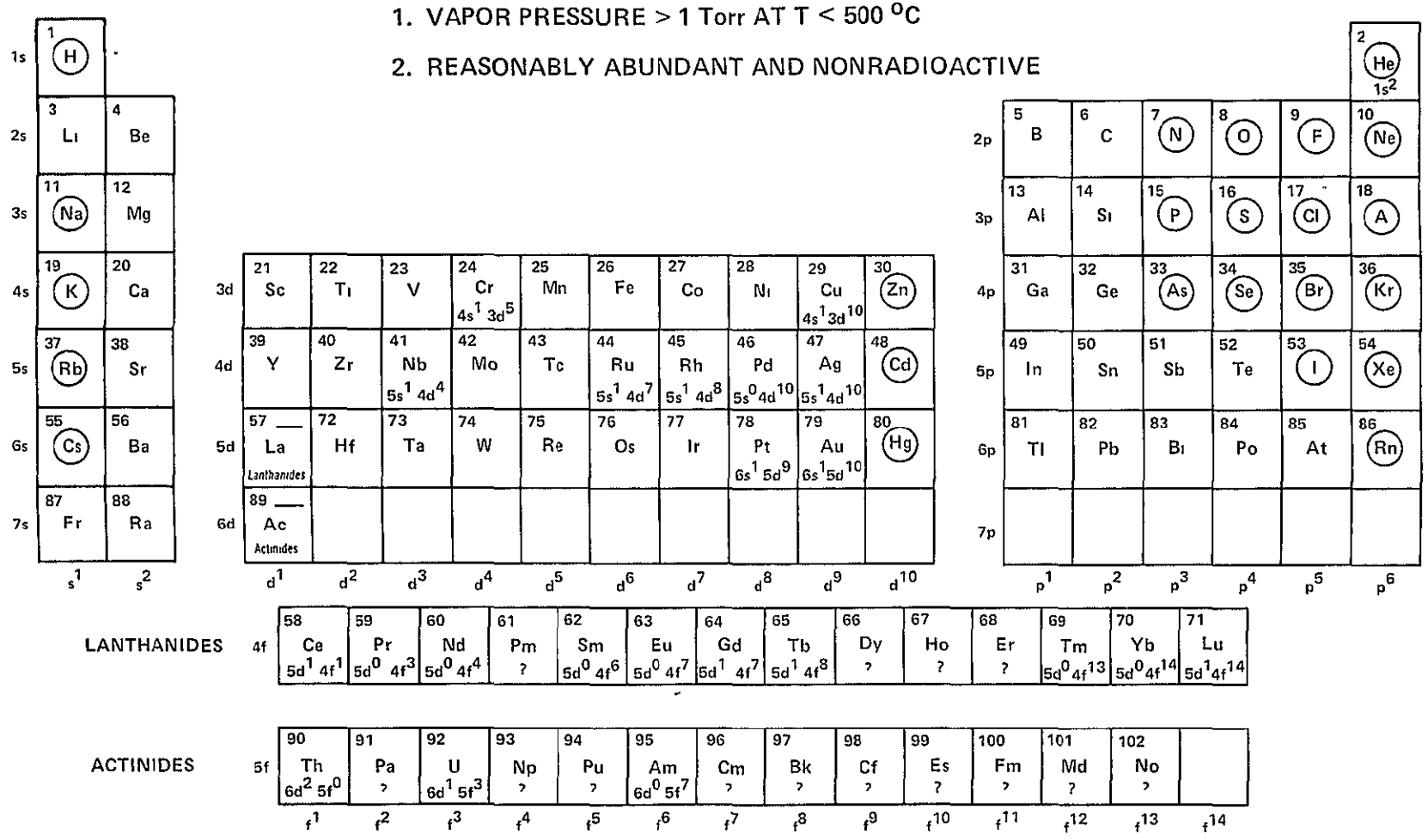

Figure II-2. Evaluation procedure applied to the periodic table.

diatomic molecule formed by the association of the element with a rare gas atom as well as on the homonuclear diatomic molecule. Figure II-3 shows potential energy curves of a heteronuclear (excimer) and homonuclear (dimer) candidate molecule representative of each group, together with a brief listing of problems and advantages associated with the use of the system as a cw excimer laser. References consulted for the survey are listed in Table II-1. A brief narrative summary of our considerations of these systems follows.

4388-6

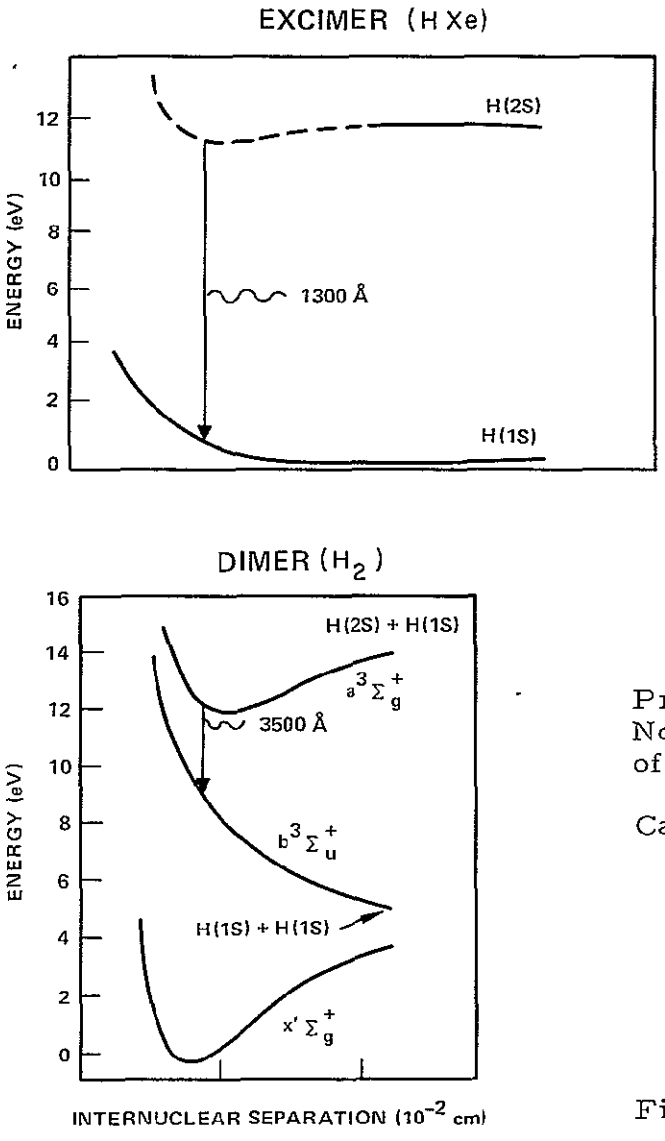

Problems: Wrong Wavelength

Candidate Systems ?: No

Problems:
No net gain due to photoionization of upper laser level

Candidate System ?: No

Figure II-3. Group 1 — Hydrogen.

Table II-1. References Consulted for the Preliminary Evaluation Task

EXIMER CANDIDATE	REFERENCE
HXe	1,2
H_2	3
Kx_e	4
K_2	5
HgXe	1
Hg_2	6, 7
Xe O	9
Xe F	10
Xe_2	11

T1937

Group I: Hydrogen — The bound-free excimer transition on the hydrogen-rare gas molecule, which correlates with the resonance transition, will lie in the vacuum ultraviolet and therefore is not a candidate system. The well-known bound-free transition at 3500 Å of H_2 has been investigated as a possible laser transition by Palmer several years ago.[3] It was found in that investigation that photoionization transitions from the upper laser level will not permit net gain to be realized on this system. The associated bound-bound transitions of H_2 are in the vacuum ultraviolet and involve well depths far too deep for the transition to be broadened into a continuum as is necessary to qualify it as an "excimer-like" transition. Hydrogen was therefore judged as not a good candidate element for this program.

Group I: Alkali Metals — The alkali metals are known to be excellent candidate excimer laser systems in both the A-X bound-unbound transition on the alkali-rare gas molecules and the A-X bound-bound transition of the alkali dimer molecules (Figure II-4). The

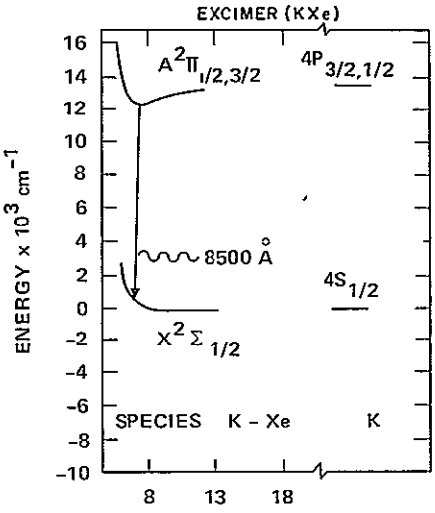

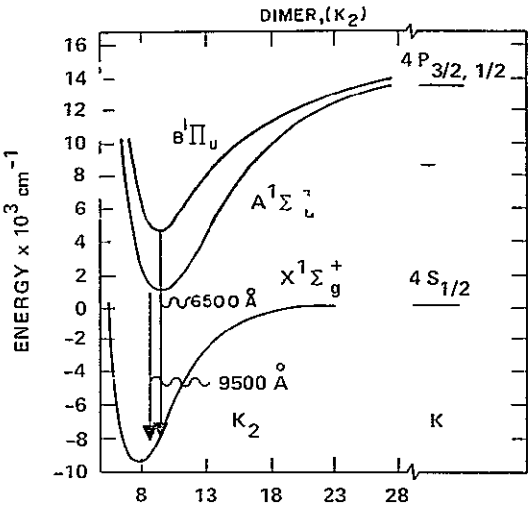

Advantages:
- Good wavelength (near IR — visible)
- Strong oscillator strength
- No competing photoexcitation processes
- Low pumping threshold (flashlamps, discharges)

Problems:
- Weak upper level binding (~0.1 eV)
- Thermal bottle-necking and dimer absorption at moderate temperatures
- High pressure alkali-rare gas mixture, difficult to handle

Candidate System: Yes

Advantages:
- Same as excimer except: potentially broader wavelength range and operation at lower pressure

Problems:
- Same as excimer except: can operate at slightly higher temperatures

Candidate System: Yes

Figure II-4. Group 1 — Alkali metals: Na, K, Rb, Cs.

dimer transition is red shifted as required and is broadened into a continuum at buffer gas pressures greater than or near one atmosphere. The excimer laser features of these systems are discussed in detail in Refs. 5 and 12. Possible problems associated with the use of these systems for cw operation are thermal dissociation of the upper levels resulting from the relatively shallow well depths and discharge instabilities caused by the metal vapor gradients. The K-Xe/K_2 system was selected as the first of the three candidate cw excimer systems to be chosen from the preliminary evaluation. Potassium was chosen in favor of the other alkalis because it requires the lowest oven vaporization temperatures of the alkalies whose excimer and dimer transitions both lie within the range of a silicon detector. Xenon is chosen in favor of the other rare gases because it forms the deepest excimer state well depth (resulting in the farthest red shift).

Zn, Cd, Hg Transition Element Subgroup — These elements have bound free transitions to the ground state on both the heternuclear rare gas molecules and on the homonuclear dimer molecules (Figure II-5).

In particular, Hg_2 has both a visible excimer transition at 4850 Å and an ultraviolet excimer transition at 3350 Å which have been recognized for some time as potential laser transitions.[6] Gain measurements carried out on the 4850 Å transition have revealed the same problem with this transition as with the H_2 excimer transition, i.e., no net gain due to vapor state absorption.[7] On the other hand, the 3350 Å transition has now been shown to exhibit net gain both with probe laser gain measurements as well as with a recent demonstration of oscillation under optical pumping by a laser.* The Hg_2 $^3l_u \rightarrow \Sigma_g$ 3350 Å excimer transition was identified as another candidate cw excimer system.

The corresponding heternuclear Hg-rare gas excimer transition is not well studied. One can anticipate a weak oscillator strength for the transition and a weak excimer state binding a relatively short

*V. Schlie, private communication.

transition wavelength, probably about 2700 Å, which will elevate the pumping power required for threshold. Thus the heteronuclear Hg-rare gas molecule is not admitted as a candidate system.

Group V and VI — The excimer and dimer transition involving the Group V elements are similar to those involving the Group VI elements (Figure II-6). Of the elements in these groups, oxygen has recently been particularly well studied as an excimer laser. The recently demonstrated XeO e-beam pumped excimer laser operates on a bound-bound molecular transition which correlates with the atomic oxygen auroral transition. While this system may be well suited to large energy storage because of the long lifetime, it is poorly suited to cw application because of the evident self-terminating nature of the transition. The transition correlating with the resonance transition on both the heternuclear excimer and homonuclear dimer molecules are in the vacuum ultraviolet and are also unsuitable for the present program.

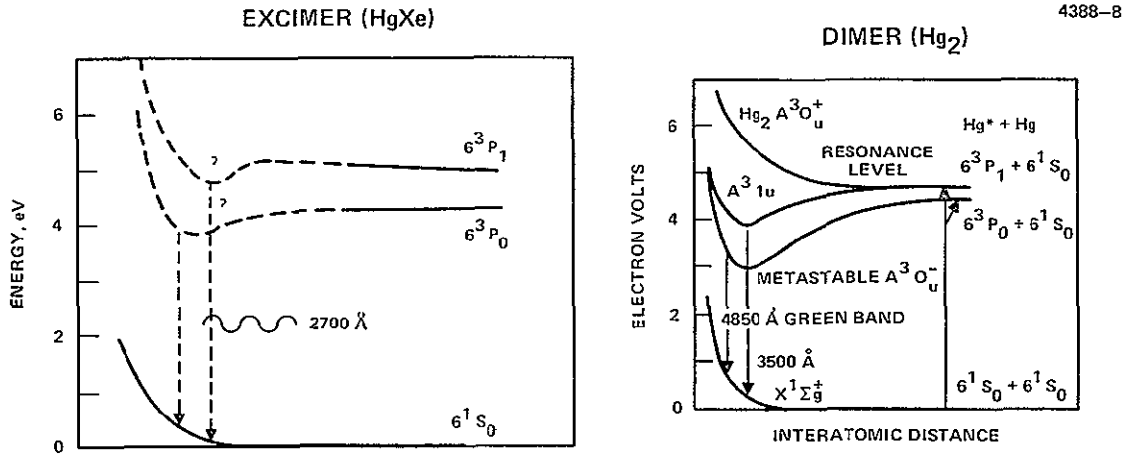

Problems:
- Weak oscillator strength
- Short wavelength
- Weak upper state binding
- Lack of data and theory on potential curves

Candidate System: No

Advantages:
- Measured gain on $^3l_u \rightarrow {}^1\Sigma_g$ transition
- Good wavelength

Problems:
- Weak upper state binding

Candidate System: Yes

Figure II-5. Transition element subgroup: Zn, Cd, Hg.

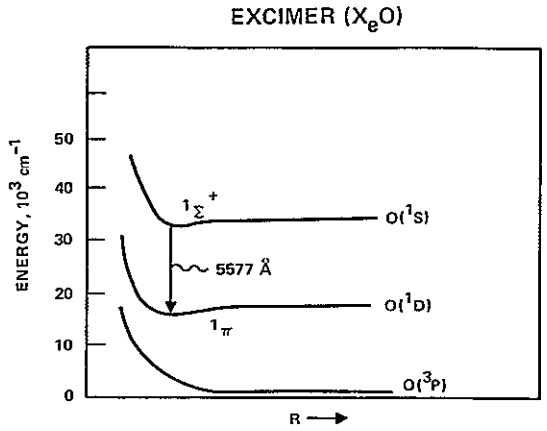

Problems:

- Extremely weak upper state binding ~0.05 eV
- Evidently a self terminating transition
- Collisionally induced dipole moment requires high pumping and high pressure

Candidate Systems: No

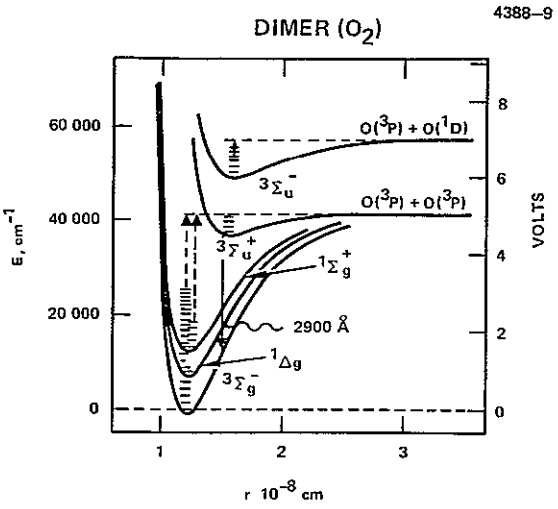

Problems:

- Lower level vibration structure Too large: cannot broaden
- Transition into a continuum and collisionally deactivate lower laser level

Candidate System: No

Figure II-6. Groups V and VI: N, P, As, O, S, Se.

Group VII — The halogen-rare gas excimer molecules appeared to be one of the most promising systems of all for use as a cw excimer laser (Figure II-7). Strong ionic-bonded excimer levels are formed by the association of a metastable rare-gas atom with a ground state halogen and the strongly allowed transition to the repulsive or weakly bound ground state is near 3000 Å. The deep excimer state well (~4 eV) will permit the use of high cw input power densities without upper state dissociation as occurs with the alkali systems. Also, because F, Br, and Cl are room temperature gases, the experimental apparatus is enormously simplified. The XeF excimer transition at 3450 Å was chosen as the candidate excimer molecule from this class because it has the longest wavelength. The halogen dimer bound-bound transition correlating with the resonance transition is not suitable because of the short wavelength and deep well depths, with vibrational level spacing too large to be broadened into a continuum.

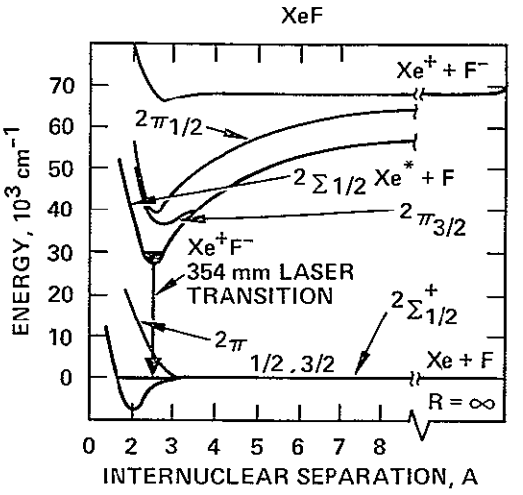

Advantages:
- Ideal wavelength
- Strong oscillator strength
- Strong upper state binding 4 eV
- Fast excimer association rates 10^{-9} cm^3 sec^{-1}
- Discharge pumping
- F, Be, Cl gasses at STP

Problems:
- Discharge stability?

Candidate System: Yes

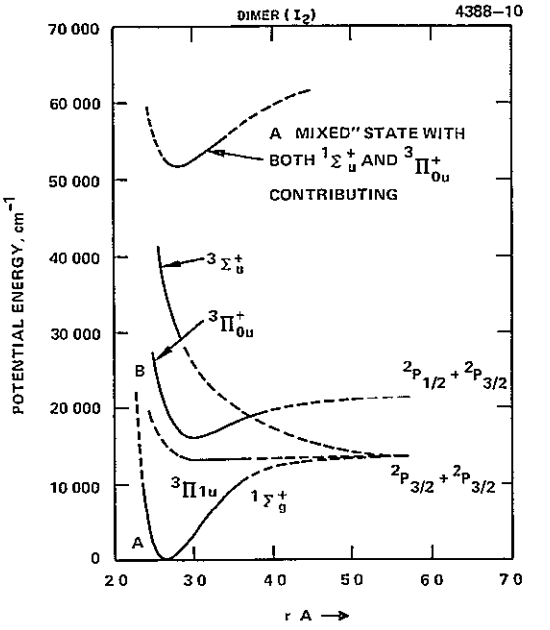

Problem:
- Same as for Group V and VI dimers

Candidate System: No

Figure II-7. Group VII: F, Br, Cl, I.

Group VIII – The rare gas dimer bound-unbound transitions are well-known laser transitions, but they lie in the vacuum ultraviolet thus requiring very large pumping thresholds, and thus are not candidate systems for this program (Figure II-8).

Having identified four specific candidate excimer molecules for detailed theoretical modeling our next task was to assemble preliminary quantitative data on the laser transition. The four candidate excimer transitions selected and their approximate wavelength are

(1) $KXe\ ^2\pi_{1/2,3/2} \rightarrow {}^2\Sigma_{1/2}$ 8500 Å

(2) $K_2\ ^1\Sigma u^+ \rightarrow {}^1\Sigma^+ g$ 10400 Å

(3) $Hg_2\ A^3 1u \rightarrow X^1\Sigma^+$ 3350 Å

(4) $XeF\ ^2\Sigma_{1/2} \rightarrow {}^2\Sigma_{1/2}$ 3450 Å

A compilation of pertinent quantitative data, including a set of potential energy curves for these transitions, are presented in Figure II-9 through II-11. References used for these data are the same as those listed in Table II-1.

B. Selection of a CW Pumping Technique

In selecting a cw pumping technique for excimer lasers it is important that one appreciates some rather general constraints concerning cw operation of an excimer laser.

The stimulated emission cross sections for visible-near visible excimer lasers average on the order of 3×10^{-17} cm^2. To sustain a practical laser gain of 1% per centimeter required for laser action it is necessary to sustain an excimer level population density of $\sim 3 \times 10^{14}$ cm^{-3}. Visible transition excimer levels have a radiative decay rate of $\sim 3 \times 10^{7}$ sec^{-1}. Discharge pumping efficiencies, from recent experiments, seem to be running near ~1%. Thus, assuming a 1 to 3 eV photon, a minimum cw input power density of $\sim 10^{4}$ to 10^{5} W/cm^3 must be provided to the excimer system for it to oscillate near threshold.

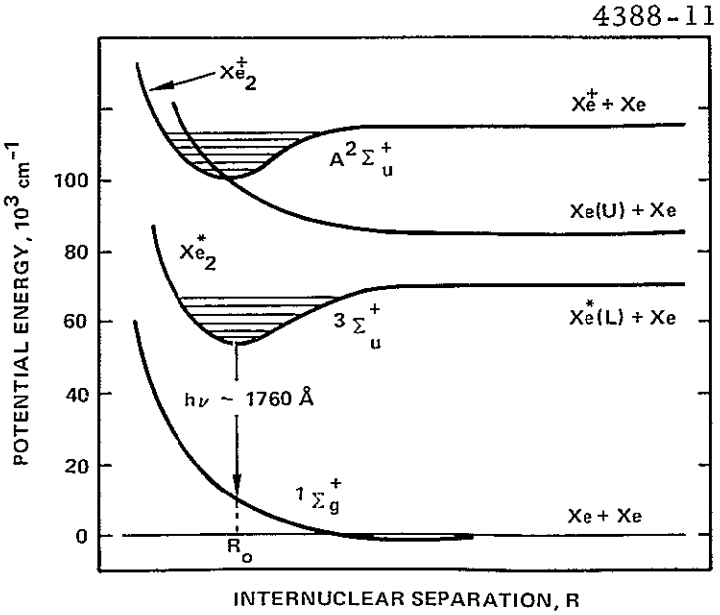

Problems:
Wrong Wavelength

Candidate Systems:
No

Figure II-8. Group VIII: He, Ne, Ar, Kr, Xe.

KXe

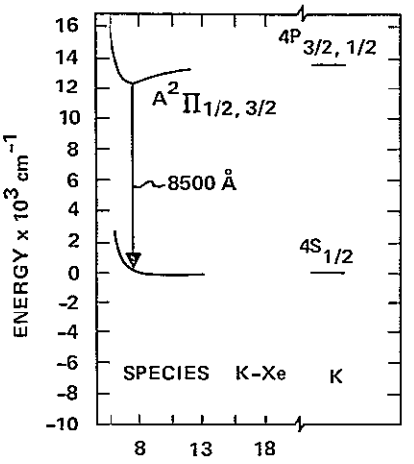

EXCIMER FORMATION REACTION

$K(P_{2/3,\,1/2}) + 2Xe \rightarrow KXe(^2\pi_{1/2,\,3/2}) + Xe$

(RATE = $\dot{8}\ 2 \cdot 10^{-32}$ cm^6 sec^{-1})

LASER TRANSITION $^2\pi_{1/2,\,3/2} \rightarrow {}^2\Sigma_{1/2}$

TRANSITION WAVELENGTH $\lambda \approx 8200 - 9000$ Å

UPPER LEVEL LIFETIME $\tau \approx 2\,7 \cdot 10^{-8}$ sec

STIMULATED CROSS SECTION $\sigma_s \approx \frac{\lambda^3}{4\pi^3 c}\left(\frac{\lambda}{\Delta\lambda}\right) \cdot \tau^{-1}$

$\approx 4 \cdot 10^{-16}$ cm^2

FRACTIONAL RED SHIFT $\frac{\nu - \nu_o}{\nu_o} \simeq 0\,092$

(EQUALS MAXIMUM Tg/Te FOR 2-TEMPERATURE INVERSION)

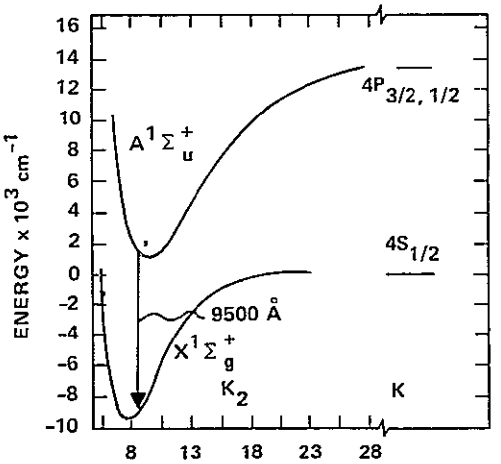

$K(P_{1/2}) + K(S_{1/2}) + X \rightarrow K_2(^1\Sigma_u^+) + X$

(RATE = $8 \cdot 10^{-30}$ cm^6 sec^{-1})

$^1\Sigma_u^+ \rightarrow {}^1\Sigma_g^+$

$\lambda \approx 9300 - 10{,}500$ Å

$\tau \approx 2\,5 \cdot 10^{-8}$ sec

$\sigma \approx 1 \cdot 10^{-16}$ cm^2

$\frac{\nu - \nu_o}{\nu_o} \approx 0\,19$

Figure II-9. Laser Transition Data: Kxe, K_2.

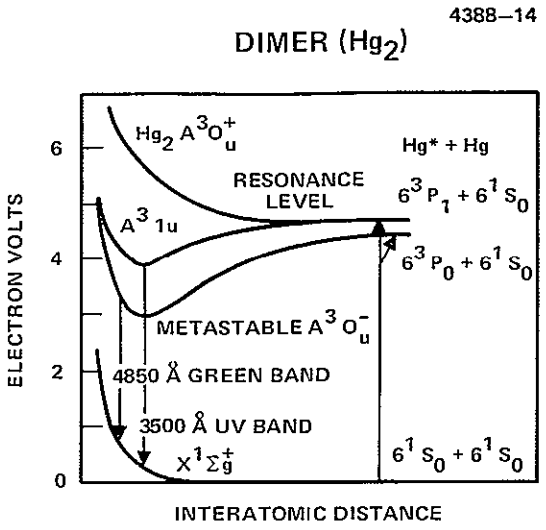

Excimer formation reaction:

$$Hg(^3P_1) + Hg(^1S_o) + X \rightarrow Hg_2(A^3 1_u) + X$$

$$(\text{Rate} \approx 1 \times 10^{-30}\ \text{cm}^6\ \text{sec}^{-1})$$

Laser transition:

$$Hg_2(A^3 1_u) \rightarrow Hg_2(X^1 \Sigma_g^+)$$

Transition wavelength:

$$\lambda \approx 3000 - 3600\ \text{Å}$$

Upper level lifetime: $\tau_u \approx 0.22\ \mu\text{sec}$

Stimulated emission cross section:

$$\sigma = 0.97 \times 10^{-18}\ \text{cm}^2$$

Fractional red shift: $\dfrac{\nu - \nu_o}{\nu_o} = 0.34$

Figure II-10. Laser Transition data: Hg_2.

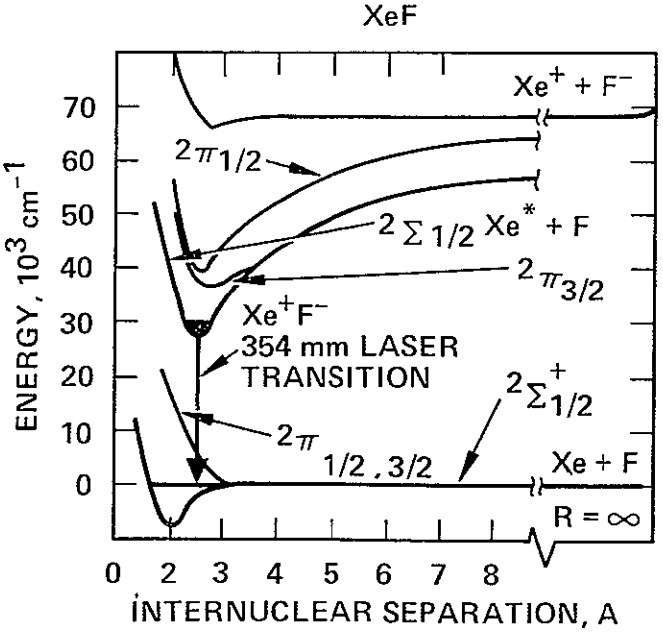

EXCIMER FORMATION REACTION

$$Xe(^3P_2) + F_2 \rightarrow XeF(^2\Sigma_{1/2}) + F$$

$$(\text{RATE} \approx 2 \cdot 10^{-9}\ \text{cm}^3\ \text{sec}^{-1})$$

LASER TRANSITION $XeF(^2\Sigma_{1/2}) \rightarrow XeF(^2\Sigma_{1/2})$

TRANSITION WAVELENGTH $\lambda \approx 3250 - 3500$ Å

UPPER LEVEL LIFETIME $\tau_u \simeq 50 \cdot 10^{-9}$ sec

STIMULATED EMISSION CROSS SECTION

$$\sigma \approx 0.5 \cdot 10^{-17}\ \text{cm}^2$$

FRACTIONAL RED SHIFT $\dfrac{\nu - \nu_o}{\nu_o} \approx 0.58$

Figure II-11. Laser transition data: XeF.

If the excimer laser is to be run in a truly steady-state cw operating mode, the power density (less the ~1% laser power extracted) must also be continuously removed from the system and the gas temperature of the active medium must be kept below ~2000°C if the population inversion is to be sustained.

The only three basic mechanisms for removing heat from the system are (1) radiation, (2) convection, and (3) conduction. We consider now the requirements for each of these mechanisms to be applied to a cw excimer laser.

1. Radiation

For radiative cooling to reach the minimum required rate of 10^4 W/cm^2 (assuming a transverse dimension of ~0.1 to 1 cm), the active medium would have to have an effective blackbody temperature of ~1 eV. An excimer system in thermal equilibrium at this temperature will not exhibit a population inversion.

2. Convection

Convective cooling using gas flow at or near atmospheric pressure is commonly used to remove heat from high average power CO_2 lasers such as the Hughes Peacemaker laser. In these devices the temperature is controlled simply by the residence time of a volume element of gas together with its specific heat: $(3/2)\,NT \cong p \cdot (d/v_{flow})$, where N is the gas density, p is the input power density, v_{flow} is the flow velocity, and d is the discharge dimension along the flow direction. It is easy to see that this technique is impractical for excimer lasers requiring a 10^5 W/cm^3 power dissipation. With an input power of this magnitude at atmospheric pressure, sonic flow conditions ($N = 3 \times 10^{19}$ cm^{-3}, $v_{flow} \cong 10^5$ cm/sec), d would have to be $\lesssim$1 mm to keep T < 1000°C. If the lower end of the above threshold pumping range is relevant (~10^4 W/cm^3), then convection may be practical. (The alkali excimer systems are expected to have pumping requirements near this latter value.)

3. Conduction

Thermal conduction of the heat to a wall in a static gas and subsequent removal by flowing coolants can achieve 10^4 W/cm^2. This will be obtained for a helium gas mixture (independent of pressure) across an assumed thermal gradient of ~1000°C, which is close to the upper limit defined by thermal bottlenecking of the population inversion and by the integrity of the wall material. For the 10^5 W/cm^3 pumping requirement, surface-to-volume ratios of ~10 will suffice for this mode of cooling. In spite of the obvious nonscalability of the thermal conduction mode, the simplicity and versatility of this mechanism motivated the choice of a capillary discharge configuration to be used for the first year phase of the program. Also, capillary discharge pumping of CO_2 waveguide lasers is now routinely used under cw conditions at pressures comparable to the pressures required of an excimer laser although under significantly lower power loading. Capillary discharges are also used for argon ion lasers under comparable power loading but at pressures lower than required for an excimer laser.

While full cw operation, i.e. for durations of minutes, is not intended, experiments with pulse lengths up to a millisecond can be carried without the need for flowing wall coolants, and this will enable one to demonstrate cw operation conditions as far as the excimer laser kinetics is concerned.

III. THEORETICAL EVALUATION

This section summarizes modeling procedures and results for discharge pumping of the XeF, KXe, and K_2 excimer systems. In the case of XeF, a comparison between the results of modeling and experiment is also presented.

A. Modeling Procedures

In each excimer system the model follows, by means of numerical integration of the appropriate rate equations, the time evolution in the discharge of several excited and ionized species, the electron and gas temperatures, and the net small signal gain coefficient near the peak of the excimer gain band. The time dependence of the circuit currents and voltages is also included with a series resistance, a series inductance, and a storage capacitor as the modeled circuit elements.

The average electron energy is computed by solving the electron energy equation,

$$J \cdot E_{disch} = \sum_i (\text{inelastic collision rate (Te)})_i \times E_i + (\text{elastic collsion rate}) \times 2 \left(\frac{Me}{M_M}\right) \times Te \qquad (3)$$

where J is the current density, E_{disch} is the discharge electric field, E_i is the inelastic energy loss for the i^{th} process, and M_M and M_e are the masses of the major component species and electron, respectively. At present, the resonance or metastable level pumping is assumed to be the dominant inelastic process contributing to the energy equation. For this reason, together with the fact that the molecular association rates which pump the upper laser levels dominate the loss of the resonance level population, the predicted efficiencies for converting discharge power to laser power is essentially the quantum efficiency of the transition that is lasing. A Maxwellian energy distribution is

assumed. The Maxwell distribution should be a fair approximation because of the dominance of two-step ionization processes over single step ionization under the considered operating conditions. Only the latter process requires electrons with energies in the tail of the distribution where a large reduction of the number of electrons from a Maxwellian distribution is known to occur.

The electron collisional rate constants are expressed in a form that results from assuming a linear rise of the cross section with energy above threshold[13]:

$$R(Te) = \frac{6 \times 10^2}{(e/m_e)/\pi} \left.\frac{d\sigma}{d\epsilon}\right|_{\epsilon_o} \left(\frac{2}{m_e} Te\right)^{3/2} \exp(-\epsilon_o/Te) \left(1 + \frac{\epsilon_o}{2Te}\right), \quad (4)$$

where ϵ_o is the threshold energy for the excitation or ionization process, $d\sigma/d\epsilon\big|_{\epsilon_o}$ is the rate of rise of cross section with energy above threshold, and m_e and e are electron mass and change.

Also, in solving eq. (3) we use an expression for the drift velocity obtained from Ref. 13:

$$V_{drift} = (2\ Te/M_M)^{1/2} \quad . \quad (5)$$

The gas temperature is calculated by assuming that all of the discharge power goes into gas heating and that heat is removed only by thermal conduction to a wall (assumed cylindrical).

$$\frac{d\ T_G}{dt} = J \cdot E_{disch}/(3/2\ [M]) - (\text{thermal conductivity}) \times \left(\frac{4.8}{\text{diameter}}\right)^2 \times (T_G - T_{wall}) \quad .$$

The discharge circuit response is governed by the familiar circuit equations.

$$V_{disch} = V_c(t) - L \times \frac{dI}{dt} - R \times I \qquad (7)$$

$$V_c(t) = V_{charge} - 1/C \int I\, dt \ , \qquad (8)$$

where V_{disch} is the discharge voltage, V_c is the capacitor voltage, V_{charge} is the initial charging voltage, I is the discharge current, and R, L, and C are the series resistance, inductance, and storage capacitance, respectively.

1. XeF System

The plasma, gas kinetic, and radiative processes included in the rate equations governing the species concentrations are presented in Tables III-1 through III-3, together with source references and in the computer code listing presented in Section 1 of the appendix. (In the listing, a B at the end of the label refers to the back reaction which is computed by detailed balancing using the appropriate equilibrium constant or Boltzmann factor for the reaction.)

The small signal gain coefficient for the XeF system is computed as follows:

$$\text{gain} = \sigma_{stim} \times ([XeF^*] - [XeFg] \times \exp(-0.074/T_G)) \qquad (9)$$

where,

$$\sigma_{stim}(P) = \frac{\lambda^3}{4\pi^2 c} \times \left(\frac{\lambda}{\Delta\lambda_{(P)}}\right) \times A_{einst} \ , \qquad (10)$$

and $\Delta\lambda$ is the measured half width of excimer band as a function of pressure, λ is the wavelength (3450 $\mathring{A}$ for XeF*), A_{einst} is the A coefficient for the transition, $[XeF^*]$ and $[XeF_g]$ are the upper and lower laser level concentrations, and the Boltzmann function accounts for gas heating effects on the population distribution in the lower level.

The plasma, gas kinetic, and radiative processes modeled for KXe/K_2 excimer systems are listed in Tables III-4 through III-6, together with source references and in the computer code listing

Table III-1. Plasma Processes Modeled for the XeF Excimer System

LABEL	PROCESS	$\frac{d\sigma}{d\epsilon_{\epsilon 0}}$	REFERENCE
R1X	$e^- + Xe \rightleftarrows Xe^* + e^-$	0.3×10^{-10} cm^2 eV^{-1} 0.05×10^{-16} cm^2 eV^{-1}	14 Rough Estimate
R37X	$e^- + Xe \rightleftarrows Xe^{**} + e^-$		
R2X	$e^- + Xe \rightarrow Xe^+ + 2e^-$	0.11×10^{-16} cm^2 eV^{-1}	14
R38X	$e^- + Xe^* \rightarrow Xe^+ + 2e^-$	5×10^{-16} cm^2 eV^{-1}	Rough Estimate
R39X	$e^- + Xe^{**} \rightarrow Xe^+ + 2e^-$	5×10^{-16} cm^2 eV^{-1}	Rough Estimate
R4X	$e^- + Xe^+_2 \rightarrow Xe^* + Xe$	$(a =) 0.346 \times 10^{-8} (T_e \text{ (eV)})^{-1/2}$ cm^6 sec^{-1}	15
R4MX	$e^- + XeM^+ \rightarrow Xe^* + M$	$(a =) 0.346 \times 10^{-8} \times (T_e \text{ (eV)})^{-1/2}$ cm^6 sec^{-1}	Rough Estimate
	Corresponding Processes for M species = Helium		
R1	$e^- + M \rightleftarrows M^* + e^-$	0.025×10^{-17} cm^2 eV^{-1}	14
R37	$e^- + M \rightleftarrows M^{**} + e^-$	0.025×10^{-17} cm^2 eV^{-1}	Rough Estimate
R2	$e^- + M \rightarrow M^+ + 2e^-$	0.08×10^{-17} cm^2 eV^{-1}	14
R38	$e^- + M^* \rightarrow M^+ 2e^-$	5×10^{-16} cm^2 eV^{-1}	Rough Estimate
R39	$e^- + M^{**} \rightarrow M^+ + 2e^-$	5×10^{-16} cm^2 eV^{-1}	Rough Estimate
R4	$e^- + M_2^+ \rightarrow M^* + M$	$(a =) 0.29 \times 10^{-8} (T_e)^{-1/2}$ cm^6 sec^{-1}	15
REL	$e^- + M \rightarrow e^- + M$	$(\sigma =) 5.5 \times 10^{-16}$ cm^2 (elastic collisions)	14
R17	$e^- + F_2 \rightarrow F^- + F$	$(\beta =) 9.1 \times 10^{-10} (T_e)^{-2.16}$ exp $(-0.165/T_e)$ cm^3 sec^{-1}	16
R28	$e^- + XeF \rightleftarrows XeF^* + e^-$	$(R_{\leftarrow} =) 2 \times 10^{-8}$ cm^3 sec^{-1}	17
DEL	$e^- + Xe^+ + \text{wall} \rightarrow Xe$	(ambipolar diffusion) $Da = 2 \times 10^3 \times (3 \times 10^{16}/[M]) \sqrt{0.03/Tg}\ Te$	13

Table III-2. Gas Kinetic Processes Modeled for the XeF Excimer System

LABEL	PROCESS	RATE COEFFICIENT	REFERENCE
G3	$M^+ + M + M \rightleftarrows M_2^+ + M$	$3.7 \times 10^{-31} \times T_G^{-1/2}$	All gas kinetic rates were obtained from Ref. 17 or from scaling arguments applied to rates given in Ref. 17
G3X	$Xe^+ + Xe + M \rightleftarrows Xe_2^+ + M$	$12 \times 10^{-31} \times T_G^{-1/2}$	
G3MX	$Xe^+ + M + M \rightleftarrows XeM^+ + M$	$5.8 \times 10^{-31} \times T_G^{-1/2}$	
G5	$M^* + M + M \rightleftarrows M_2^+ + M$	$12 \times 10^{-33} T_G^{-1/2}$	
G5X	$Xe^* + Xe + M \rightleftarrows Xe_2^* + M$	$15 \times 10^{-32} T_G^{-1/2}$	
G5MX	$Xe^* + M + M \rightarrow XeM^* + M$	$47 \times 10^{-33} T_G^{-1/2}$	
G13	$M^* + Xe \rightarrow Xe^+ + e^- + M$	$29 \times 10^{-10} T_G^{-1/2}$	
G14	$M_2^* + Xe \rightarrow Xe^+ + e^- + M$	$29 \times 10^{-10} T_G^{-1/2}$	
G18X	$Xe^* + F_2 \rightarrow XeF^* + F$	$34.7 \times 10^{-10} \times T_G^{-1/2}$	
G20X	$Xe_2^* + F_2 \rightarrow XeF^* + F + Xe$	$35 \times 10^{-10} \times T_G^{-1/2}$	
G22	$M^+ + F^- \rightarrow M^* + F$	$5 \times 10^{-7} T_G^{-1/2}$	
G22X	$Xe^+ + F^- \rightarrow Xe^* + F$	$17 \times 10^{-7} T_G^{-1/2}$	
G23	$M^+ + F^- M \rightarrow MF^* + M$	$3 \times 10^{-25} T_G^{-1/2}$	
G23X	$Xe^+ + F^- + M \rightarrow XeF^* + M$	$12 \times 10^{-25} T_G^{-1/2}$	
G24	$M_2^+ + F^- \rightarrow M_2^* + F$	$5 \times 10^{-7} T_G^{-1/2}$	
G24X	$Xe_2 + F^- \rightarrow Xe_2^* + F$	$17 \times 10^{-7} T_G^{-1/2}$	
G25	$M_2^+ + F^- \rightarrow Xe_2^* + F$	$3 \times 10^{-25} T_G^{-1/2}$	
G25X	$Xe_2^+ + F^- + M \rightarrow XeF^* + F + M$	$12 \times 10^{-25} T_G^{-1/2}$	
G27X	$XeF^* + F_2 \rightarrow XeF + F + F$	$46 \times 10^{-10} T_G^{-1/2}$	
G31	$M^* + M^* \rightarrow M_2^+ + e^-$	$10 \times 10^{-10} T_G^{-1/2}$	
G31X	$Xe^* + Xe^* \rightarrow Xe_2^+ + e^-$	$30 \times 10^{-10} T_G^{-1/2}$	
G31MX	$Xe^* + M^* \rightarrow XeM^+ + e^-$		
G32	$M^* + M_2^* \rightarrow M_2^+ + M + e^-$	$10 \times 10^{-10} T_G^{-1/2}$	
G32X	$Xe^* + Xe_2^* \rightarrow Xe_2^+ + Xe + e^-$	$20 \times 10^{-10} T_G^{-1/2}$	
G33	$M_2^* + M_2^* \rightarrow M_2^+ + 2M + e^-$	$10 \times 10^{-10} T_G^{-1/2}$	
G33X	$Xe_2^* + Xe_2^* \rightarrow Xe_2^+ + 2Xe$	$30 \times 10^{-10} T_G^{-1/2}$	

Table III-2. Continued

LABEL	PROCESS	RATE COEFFICIENT	REFERENCE
G33MX	$XeM^* + XeM^* \rightarrow XeM^+ + M + Xe + e^-$	$20 \times 10^{-10} T_G^{1/2}$	
G34	$M^* + XeF^* \rightarrow XeM^* + F + e^-$	$10 \times 10^{-10} T_G^{1/2}$	
G34X	$Xe^* + XeF^* \rightarrow Xe_2^+ + F + e^-$	$30 \times 10^{-10} T_G^{1/2}$	
G35X	$Xe_2^* + XeF^* \rightarrow Xe_2^+ + XeF + e^-$	$30 \times 10^{-10} T_G^{1/2}$	
G35MX	$XeM^* + XeF^* \rightarrow XeM^+ + XeF + e^-$	$20 \times 10^{-10} T_G^{1/2}$	
G40	$F + F + M \rightarrow F_2 + M$	$1 \times 10^{-32} T_G^{1/2}$	
G41	$F + Xe + M \rightleftarrows F\,Xe + M$	$2 \times 10^{-32} T_G^{1/2}$	
G44	$F + Xe^* + M \rightarrow XeF^* + M$	$6 \times 10^{-32} T_G^{1/2}$	
	Equilibrium Constants for Processes 3X, 5X, and 41		
K3X		$1 \times 10^{-23} \exp(0.6/T_G)$	Rough Estimate
K5X		$1 \times 10^{-23} \exp(1.5/T_G)$	Rough Estimate
K41		$1 \times 10^{-23} \exp(0.074/T_G)$	Rough Estimate

T1944

Table III-3. Radiative Processes Modeled for the XeF Excimer System

LABEL	PROCESS	RATE	REFERENCE
AX2	$Xe^{**} \rightarrow Xe + h\upsilon$	$4 \times 10^{7}\ sec^{-1}$	Rough Estimate.
AXED1	$Xe_2^{*} \rightarrow Xe + Xe + h\upsilon$	$4 \times 10^{7}\ sec^{-1}$	17
AXEF	$XeF^{*} \rightarrow XeF + h\upsilon$	$2 \times 10^{7}\ sec^{-1}$	17
AMX	$XeM^{*} \rightarrow Xe + M + h\upsilon$	$10 \times 10^{7}\ sec^{-1}$	Rough Estimate
AM_2	$M^{**} \rightarrow M + h\upsilon$	$32 \times 10^{7}\ sec^{-1}$	Rough Estimate
AMD1	$M_2^{*} \rightarrow M + M + h\upsilon$	$32 \times 10^{7}\ sec^{-1}$	Scaled from Xe_2^{*} value in Ref 17

T1945

Table III-4. Plasma Processes Modeled for the KXe/K_2 Excimer System

LABEL	PROCESS	$\frac{d\sigma}{dt_{\epsilon 0}}$	REFERENCE
RPI	$e^{-} + K \rightarrow K^{+} + 2e^{-}$	$0\,5 \times 10^{-16}\ cm^{2}\ eV^{-1}$	14
RPI	$e^{-} + K \rightleftarrows K^{*} + e^{-}$	$6 \times 10^{-15}\ cm^{2}\ eV^{-1}$	14
RPII	$e^{-} + K^{*} \rightarrow K^{+} + 2e^{-}$	$5 \times 10^{-16}\ cm^{2}\ eV^{-1}$	Rough Estimate
RECP	$e^{-} + K^{+} + e^{-} \rightarrow K^{*} + e^{-}$	$(\alpha =)\ 2\,28 \times 10^{-26}\ (T_e)^{-4\,39}\ cm^{6}\ sec^{-1}$	15 (cesium)
RECPX	$e^{-} + K\ Xe^{+} \rightarrow K^{*} + Xe$	$(\alpha =)\ 3\,3 \times 10^{-5}\ (T_e)^{-0\,67}\ cm^{3}\ sec^{-1}$	Rough Estimate
RECPD	$e^{-} + K_2^{+} \rightarrow K^{*} + K$	$(\alpha =)\ 3\,3 \times 10^{-5}\ (T_e)^{-0\,67}\ cm^{3}\ sec^{-1}$	Rough Estimate
CEL	$e^{-} + Xe \rightarrow e^{-} + Xe$	$(\sigma =)\ 5\,5 \times 10^{-16}\ cm^{2}$	14

T1941

Table III-5. Gas Kinetic Processes Modeled for the KXe/K_2 Excimer System

LABEL	PROCESS	EQUILIBRIUM CONSTANTS OR RATE COEFFICIENT	REFERENCE
KXEX	$K + 2\,Xe \rightleftarrows K\,Xe + Xe$	$2.2 \times 10^{-23} \exp(-0.05/T_G) cm^3$	Rough Estimate
KXDI	$K + K + Xe \rightleftarrows K_2 + Xe$	$1.8 \times 10^{-22} \exp(0.56/T_G) cm^6$	5
KAXI	$K^* + 2\,Xe \rightleftarrows K\,Xe^* + Xe$	$2.2 \times 10^{-23} \exp(0.074/T_G) cm^3$	18
GPD	$K^* + K + Xe \rightleftarrows K_2{}^* + Xe$	$8 \times 10^{-30}\ cm^6\ sec^{-1}$	5
KAXI	$K^+ + 2\,Xe \rightleftarrows K\,Xe^+ + Xe$	$2.2 \times 10^{-23} \exp(0.074/T_G)\ cm^3$	18
KADI	$K^+ + K + Xe \rightleftarrows K_2{}^+ + Xe$	$6.5 \times 10^{-23} \exp(0.735/T_G)\ cm^3$	Rough Estimate
CDIF	Heavy particle elastic cross section	$1 \times 10^{-15}\ cm^2$	Rough Estimate

T1942

Table III-6. Radiative Process Modeled for the KXe/K_2 Excimer System

LABEL	PROCESS	RATE	REFERENCE
AT	$K^* \rightarrow K + h\upsilon$	Trapped Rate (computed)	20
AP	$KXe^* \rightarrow KXe + h\upsilon$	$3.69 \times 10^7\ sec^{-1}$	19
AP	$K_2{}^* \rightarrow K_2 + h\upsilon$	$3.69 \times 10^7\ sec^{-1}$	Rough Estimate

T1943

presented in Section 2 of the Appendix. In this system, under the conditions we consider ($[Xe] \cdot 1 \times 10^{20}$ cm^{-3}) the gas kinetic rates dominate over electron collisional rates in controlling the population of the molecular states. We therefore assume thermal equilibrium at the gas temperature to be maintained between the molecular states and their dissociation products. An exception is the A state of K_2 for which radiative losses are included since they can compete with the dissociation rate.

The small signal gain coefficient for the KXe/K_2 system is computed from the quasi-state theory of line broadening as in Ref. 21:

$$\text{gain}(\lambda) = \sigma_{\text{stim, ex}}(\lambda) \left\{ [KXe^*] \times \frac{\exp(-V_{A,Ex}(\lambda)/T_G)}{(K_{\text{eq A, Ex}} \times 3/2} - 2 \times [K] \times [Xe] \times \exp(-V_{x,Ex}(\lambda)/T_G) \right\}$$

$$+ \sigma_{\text{stim, Di}}(\lambda) \left\{ [K_2^*] \times \frac{\exp(-V_{A,Di}(\lambda)/T_G)}{(K_{\text{eq A, Di}} \times 12)} - 0.25 \times [K]^2 \times \exp(-V_{x,Di}(\lambda)/T_G) \right\} \quad (11)$$

$$\sigma_{\text{stim}}(\lambda)_{\substack{Ex \\ Di}} = (A_E/2c) \times \quad ^2 \times R^2_{\substack{Ex \\ Di}} \times \left. \frac{dR(\lambda)}{d\nu} \right|_{\substack{Ex \\ Di}} , \quad (12)$$

where λ and ν are the transition wavelength and frequency, c is the speed of light, $R_{\substack{Ex \\ Di}}$ is the internuclear separation on the excimer or dimer band corresponding to the wavelength, λ, A_E is the Einstein A coefficient assumed equal to the resonance line at coefficient for both the excimer and dimer bands, $V(\lambda)$s are the potential energies of the molecular state measured relating to their dissociation products, and $K_{eq,A,Ex}$ and $K_{eq,A,Di}$ are the equilibrium constants for the excimer and dimer A states. This notation follows that used in Ref. 21.

The computer program listings in the appendix show how the coupled rate equations governing all of the above processes are integrated numerically using a time step chosen by the user and altered, if desired, during the course of the computer run. The computer program is written for the PDP10 computer.

B. Results and Discussion

1. Discharge Stability Considerations

Discharge stability considerations are, of course, of paramount important in considering cw operation of a discharge pumped excimer laser. There is a wide range of discharge instabilities that can occur in discharge pumped lasers. Many of these instabilities, such as the various thermal instabilities, have relatively slow growth rates and can be stabilized by simply controlling the gas temperature or gas flow as is necessary in any case discussed above. However, there is one fairly fast growing instability that is a particular problem with discharge pumped excimer lasers and deserves special discussion. This is the two-step ionization instability which results from the high metastable or resonance level population required in these systems. Collisional ionization of these levels dominates the ionization of an excimer system pumped over laser threshold and leads to a quadratic increase of the ionization rate with electron density. The ionization is thus unstable if the electron loss rate varies only linearly with electron density as is the case for attachment or diffusion-controlled discharges. Recombination controlled discharges are only marginally stable against two-step ionization instabilities.

There are only four basic ways to achieve excimer laser threshold without encountering the above instability:

1. Establish the threshold input power in the discharge in a time that is short compared with the growth time of the instability (TEA and Bloom line fast discharge devices).

2. Operate the discharge at below avalanche E/P values where the instability does not occur. This requires the use of an external source of ionization.

3. Stabilize the instability with a current limiting element in the discharge circuit, such as a ballast resistor.

4. Operate the discharge in a regime which depletes the ionizing species thereby saturating the two-step ionization rate.

Approach No. 1 is a demonstrated successful means of obtaining discharge pumped laser action in the XeF and KrF excimer systems. It is clearly inapplicable to cw operation. Approach No. 2, using an electron beam as the external source of ionization, is an approach currently being pursued elsewhere for high average power operation on the rare gas monohalide excimer lasers. It is considered marginal at best for cw operation because of thermal loading of the e-beam foil window.

Approach No. 3, of course, has been used for decades to stabilize gas discharges. It is the approach chosen for this program for stabilizing the XeF capillary discharge and is the anticipated approach (through the use of distributive resistive electrode) to stabilizing the transverse XeF discharges in the forthcoming phase of the program.

Approach No. 4 can be used for the alkali excimer system because required alkali concentration (which is the ionized species) is enough to permit ionization saturation effects to occur.

Approaches 3 and 4 are the chosen mechanism for stabilizing the two-step ionization instability in this program. The numerical modeling results, in fact, dramatically reveal the stabilizing effects of both of these mechanisms. In the case of ballast resistor stabilization a simple model is presented below which exposes more clearly the basic physical requirements for this method of stabilizing the two-step ionization instability.

The two-step ionization instability in an excimer laser is described by the following coupled rate equations for electrons and the metastable (or resonance) level population:

$$\frac{d}{dt} n_e = R_i' n^* n_e - \beta n_e \tag{13}$$

$$\frac{d}{dt} n^* = R_m n_e - n^*/\tau \quad , \tag{14}$$

where n^* and n_e are the metastable (or resonance) level concentration and electron concentration, respectively, R_i is the rate constant (per n^*) for ionization of the metastable, R_m is the production rate constant for metastables, β is the linear loss rate of electrons, and τ is the effective lifetime of the metastable.

The steady-state solution to these equations is

$$n_{e_o} = \beta/R_i R_m \tau \tag{15}$$

and

$$n_o^* = R_m \tau n_{e_o} \quad . \tag{16}$$

This solution is unstable as shown by linearizing eqs. (13) and (14) with respect to the perturbed solution:

$$n_e = n_{e_o} + n_e'(t) \exp(\alpha t) \tag{17}$$

and

$$n^* = n_o^* + n^{*'}(t) \exp(\alpha t) \quad . \tag{18}$$

This procedure gives

$$\alpha = 1/2 \times 1/\tau \times \left[-1 \pm \sqrt{1 + 4\beta\tau}\right] . \tag{19}$$

Thus the steady state solutions (15) and (16) are unstable with a growth rate given by the positive root for α. However, if there is a ballast

resistor in the discharge circuit, the rate constants R_m and R_i will be decreasing functions of n_e, and one must include this dependence in the linearized stability analysis. The most sensitive dependence will be on R_m since it contains the most strongly varying Boltzmann factor ($\exp(-E_m/Te)$) compared with $\exp(-(E_i - E_m)/Te)$ for R_i' where E_i and E_m are ionization and metastable level energies, respectively. Thus, in the perturbation analysis of eqs. (13) and (14) we also write

$$R_m = R_{m_o} + \frac{d R_m}{d n_e} n_e \quad . \tag{20}$$

After collecting terms linear in n_e' as before, the solution for will now have an added term:

$$\alpha = 1/2\left[1/\tau \quad -1 \pm \sqrt{1 + 4\beta\tau \left(1 + \frac{(dR_m/dn_e)}{Rm_o} n_{e_o}\right)}\right]. \tag{21}$$

To determine $dR_m/d\, n_e$ we now make use of the fact that under conditions required for pumping excimer lasers, the dominant electron energy loss is due to the inelastic collisional pumping of the metastable level. Thus the energy conservation relation for electrons can be written approximately as

$$J \times E = n_e R_m E_m \quad , \tag{22}$$

where J and E are the current density and field in the discharge. If there is a ballast resistor in the circuit this equation can be written

$$eN_e V_d(V - IR)/\ell = n_e R_m E_m \tag{23}$$

where V is the maintained power supply voltage, I is the current, R is the ballast resistance, ℓ is the discharge gap, and V_d is the drift velocity.

Using $I = n_e V_d$ eA where A is the discharge area and e the electron charge we can write

$$\frac{d R_m}{d n_e} = - \frac{V_d}{\ell E_m} RA V_d e = - \frac{R_{m_o} RA V_d e}{V - IR} = \left(- \frac{R_{m_o}}{n_{e_o}} \right) x \left(\frac{RI}{V - IR} \right). \quad (24)$$

Using eq. (21) we see that stability is achieved if $RI/(V - IR) \geq 1$, i.e., the drop across the ballast resistor must be equal to or greater than the discharge voltage. The onset of discharge stability when this condition is met is revealed in the numerical modeling for the XeF system as well as in the observed current voltage waveforms in the capillary discharge pumped XeF experiments.

2. Modeling Results for the Capillary Discharge Pumped XeF System

A typical result of the numerical integration of the modeling equations governing discharge pumping of the XeF excimer system is shown in Figure III-1. The curves are discharge current and voltage and the excimer level population density versus time. In the inset of the figure a typical experimental observation of the same temporal profile is shown for comparison.

As can be seen, the qualitative features of experimentally observed waveforms are well reproduced by the theory. The time scale over which these features occur is shorter for the theoretical case because of the high currents reached in modeling. In both the experimental and theoretical waveforms three distinct phases of the temporal development are revealed. An initial transient phase, an intermediate steady state phase and a final terminated-fluorescence phase.

The initial phase in which the excimer fluorescence reaches its peak value is the transient period during which the discharge field and electron temperature attain their peak values. These values are limited primarily by the discharge circuit inductance. This is the discharge phase during which XeF excimer laser action is being achieved in the TEA and bloomline fast discharge devices. While it may be possible to achieve laser action in the capillary discharge during this

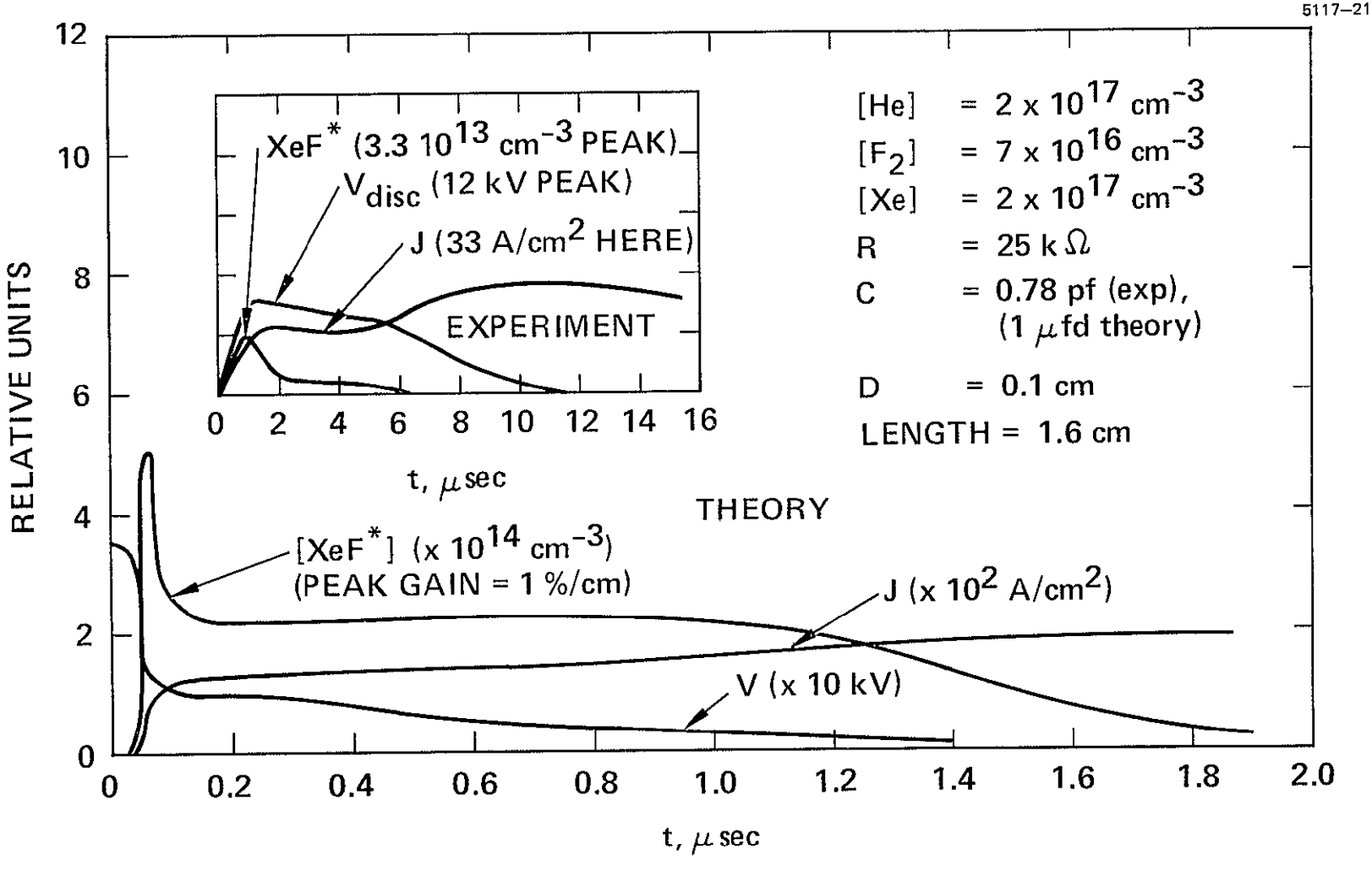

Figure III-1. Capillary discharge pumped XeF excimer results: theory versus experiment.

phase through optimization of the discharge risetime, what happens during this transient phase is immaterial for cw operation, and thus we give this possibility no further consideration.

The intermediate steady-state phase of the discharge is the desired cw operating regime. Although not shown in the plot, the modeling results confirm that the gas temperature rise has been stabilized by thermal conduction to the wall during this phase. Also, as can be seen, the discharge is stable during this period, the two-step ionization instability having been stabilized by the 25 kΩ ballast resistor. The magnitude of the excimer fluorescence and discharge current during this and the preceding transient phase of the discharge are lower in the experiment than those predicted by theory by factors of ten. The fluorescence during this phase would have to be increased by about a factor of ten to give a practical laser gain coefficient of ~1% per centimeter.

For cw operation a more serious problem than the low value of observed fluorescence is the observed and predicted termination of fluorescence. This occurs in both the experimental and theoretical cases long before the discharge capacitor is drained and has been traced to the consumption of fluorine by the XeF excimer level pumping reaction itself (reaction G18X). We have identified, therefore, a fundamental constraint to cw operation of an XeF excimer laser. The basic requirements for overcoming the fluorine consumption problem can be appreciated by examining the rate equation for F_2. Replenishment of F_2 at the required rate by gas flow is not practical in a capillary tube so the rate equation is written for a static gas.

$$\frac{d[F_2]}{dt} = \Gamma_{diss}[Xe^*][F_2] - \Gamma_{rec}[F]^2[He] = 0$$

$$\| \quad 4 \times 10^{21}\ cm^{-3}\ sec^{-1} \text{ (for 0.2\%/cm gain)} \qquad (25)$$

and

$$\Gamma_{rec} \quad 1.5 \times 10^{-33}\ cm^3\ sec^{-1} \ .$$

To achieve a minimum practical laser gain of 0.2%/cm the pumping rate (consumption rate) must be $\geq 4 \times 10^{21}$ cm^{-3} sec^{-1}. For molecular recombination to stabilize the F_2 concentration at $\sim[F_2] \approx 10^{17}$ cm^{-3} where stable discharge operation is presently being achieved (higher F_2 concentration will lead to impractically high discharge voltages to overcome the higher attachment loss), a 50% dissociation fraction and a third body concentration of $\sim 3 \times 10^{20}$ cm^{-3} is required. In principle, the requirement of a high buffer gas pressure is not incompatible with the operation of cw capillary discharge pumping of this excimer system since neither thermal conduction nor the two-step ionization instability is dependent on buffer gas pressure. Experimentally, however, attempts to elevate the buffer gas (helium) pressure above ~100 Torr have led to filamenting of the discharge.

The F_2 consumption problem and consequent requirement of operating at 1 to 10 atm of buffer gas pressure at present is the most outstanding problem for cw capillary discharge pumping of the XeF excimer system. Conclusive evaluation of this problem is expected to be completed in the early phase of the second year's contract period for this program.

3. Modeling Results for the Capillary Discharge Pumped KXe/K_2 Excimer System

The results of three computer runs of the capillary discharge pumped KXe/K_2 model are presented in Figures III-2 and III-3. The series inductance, L, is assumed equal to zero in these runs.

The two results presented in Figure III-1 are for a discharge through a 10 atm K-Xe mixture at two different temperatures. As is the case for optical pumping, the lower temperature result shows most of the gain occurring on the excimer band (8500 Å), while the higher temperature case shows the highest gain occurring on the dimer band. In both cases the model predicts that a fairly high E/N value of $\sim 10^{-11}$ $V/(cm \times [K]\ cm^{-3})$ is required to give practical gain coefficients of ~1% cm.

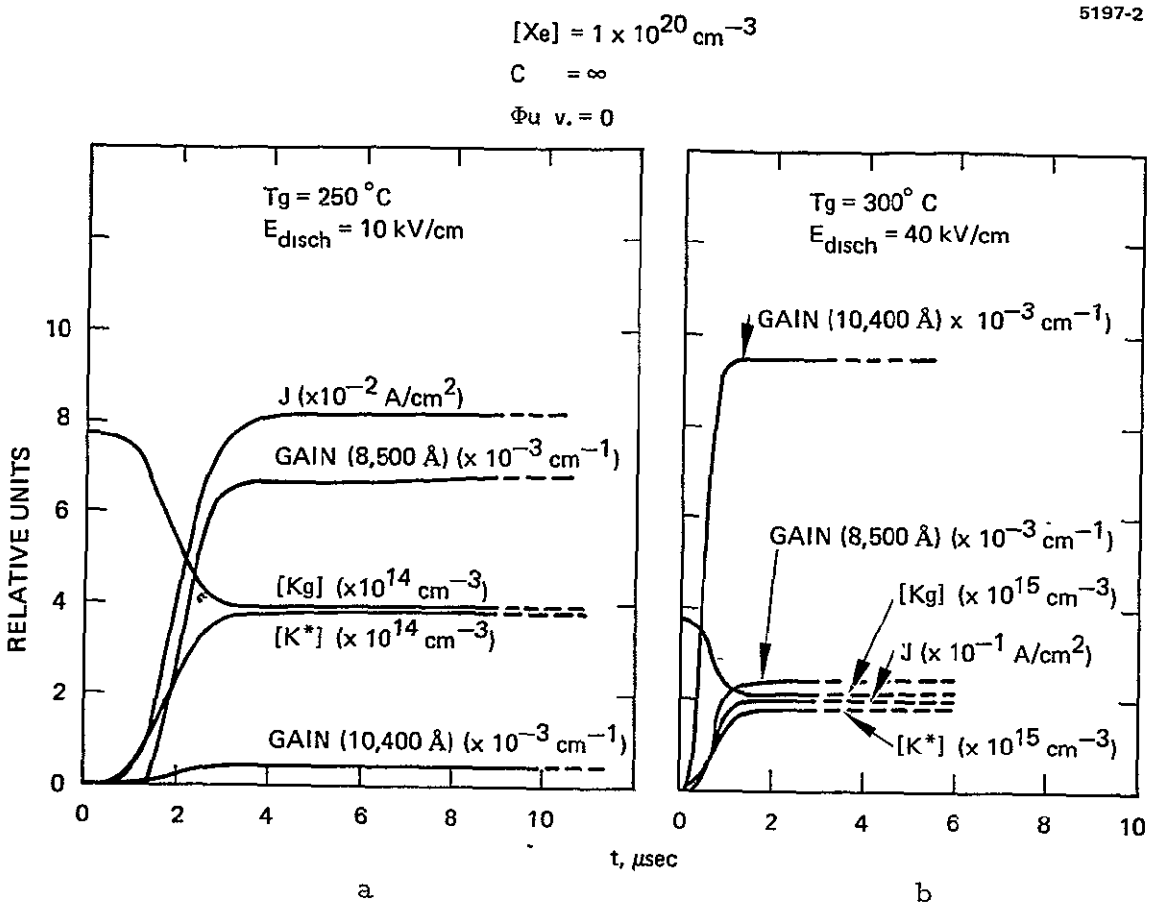

Figure III-2. Theoretical modeling results for avalanche sustained discharge pumping of the K-Xe/K_2 system. (a) Low temperature results. (b) High temperature results.

The results in Figure III-2 are for an infinite storage capacitance and no ballast resistor. These results illustrate an important feature of the discharge kinetics. Unlike the rare gas monohalides the alkali rare gas discharge in the modeling appears to be intrinsically stable against ionization instabilities. This stability is apparently due to two causes: first, the ground state potassium population is depleted during the discharge, resulting in a saturation of the ionization and, to a lesser extent, the discharge is recombination stabilized rather than attachment stabilized. (Ambipolar diffusion is negligible at these pressures.

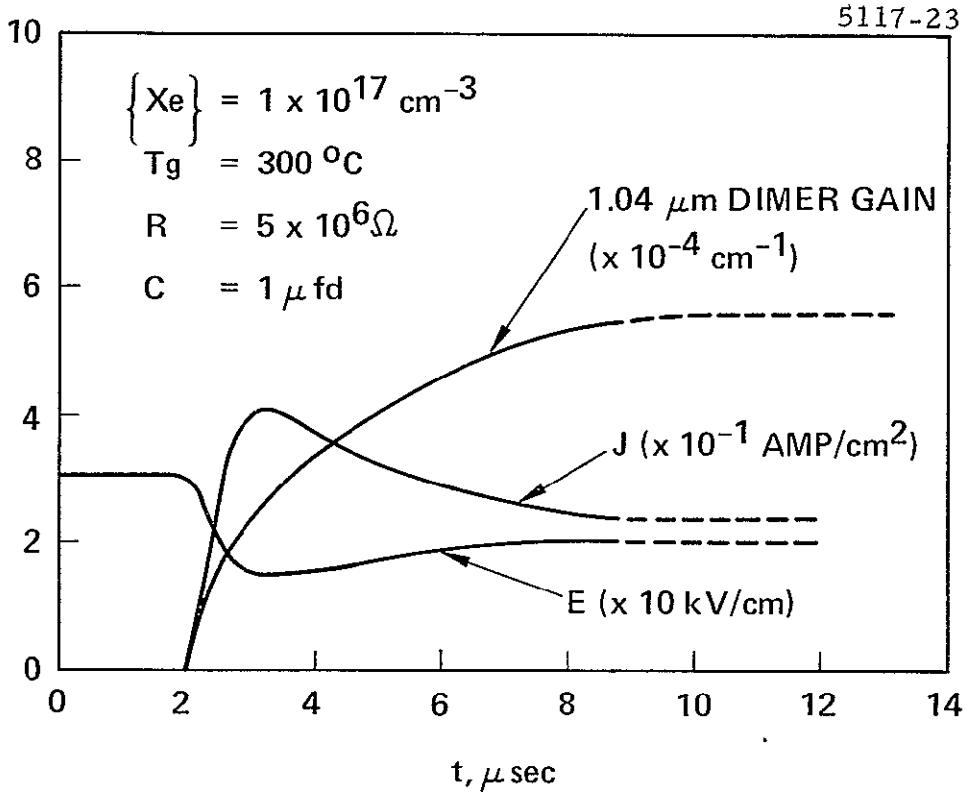

Figure III-3. Capillary K_2 pumping: low pressure case.

The low pressure modeling results in Figure III-2 show gain only on the dimer band, of course, and the magnitude of the gain coefficient is an order of magnitude lower than that of the high pressure case under otherwise similar conditions because of the reduced contribution of the three-body resonance level associations reaction (reaction GPD). Also, in the modeling, a ballast resistor is necessary to stabilize the ionization instability, probably because the low pressure discharge is wall stabilized (linear loss rate of electrons) rather than recombination stabilized as in high pressure case. However, it is not yet certain that a divergence of the numerical integration procedure is not involved in this case.

In all three cases modeled gas temperature is adequately controlled by thermal conduction to the capillary tube wall, as originally anticipated in the preliminary evaluation phase of the program.

IV. LABORATORY APPARATUS

The objective of this task is to design and fabricate experimental apparatus for the purpose of evaluating the potential laser systems recommended from our theoretical studies. As discussed in Sections II and III, this analytical work identified the potassium-xenon (KXe), or argon, excimer, potassium dimer (K_2), and xenon fluoride (XeF) as promising laser species to meet the NASA high-power laser requirements for continuous operation in the visible wavelength spectral region. Electrical discharge excitation in a small bore capillary tube was also predicted to be the best pumping technique to use for preliminary experimental evaluation of these systems.

Both the alkali excimer-dimer and the rare gas halides pose significant materials problems which must be considered in the design of apparatus. Potassium is chemically reactive with many materials and must be heated to ~300°C to achieve sufficient density for laser oscillation. Molecular fluorine is difficult to handle because it is one of the most powerful oxidizing agents known. With these factors in mind the gas handling apparatus shown in Figure IV-1 was designed and fabricated for use with the XeF laser system. This apparatus is constructed primarily of stainless steel tubing and incorporates stainless steel packless valves and fluorine compatible pressure gauges. The entire system was passivated with fluorine-helium mixtures and pure fluorine prior to use for discharge measurements. Nitrogen trifluoride (NF_3) presents less of a materials problem and was also used in this apparatus as a fluorine source for reaction with excited xenon atoms.

The discharge tube and electrical pulse circuit are shown photographically in Figure IV-1 and schematically in Figure IV-2. Stainless steel cylindrical cavity electrodes as shown in these figures were found to be more satisfactory than simple tunsten pin electrodes which were used in our first XeF discharge experiments. The discharge tube was situated within an optical cavity as shown in Figure IV-1. Alignment of the optical cavity was achieved with the use of a He-Ne laser and conventional alignment techniques.

M11457

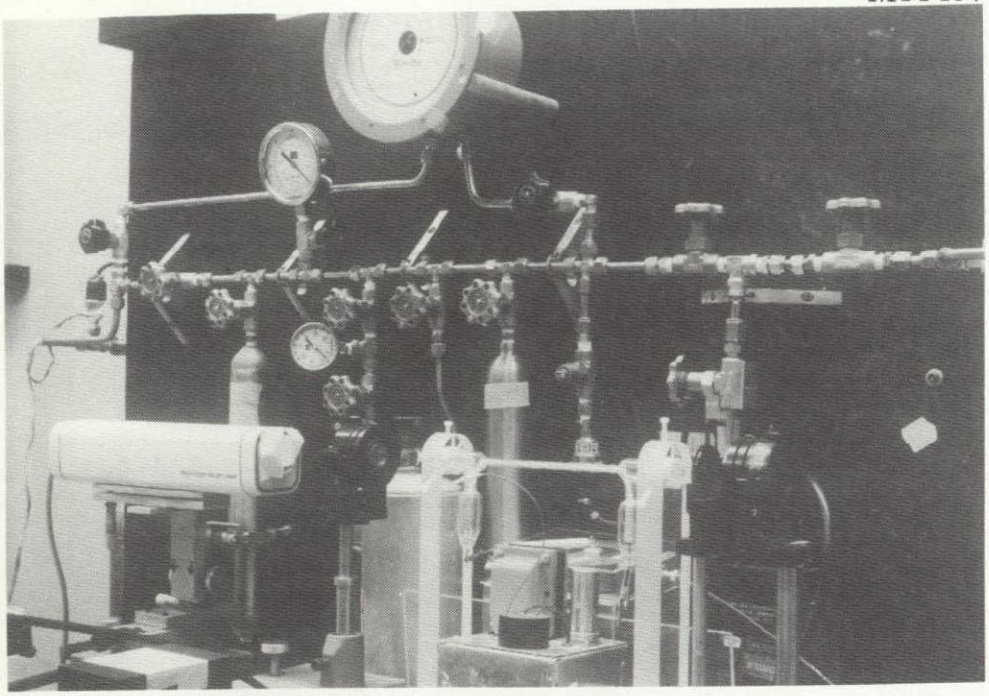

Figure IV-1. Rare-gas halide capillary discharge laser apparatus.

5117-34

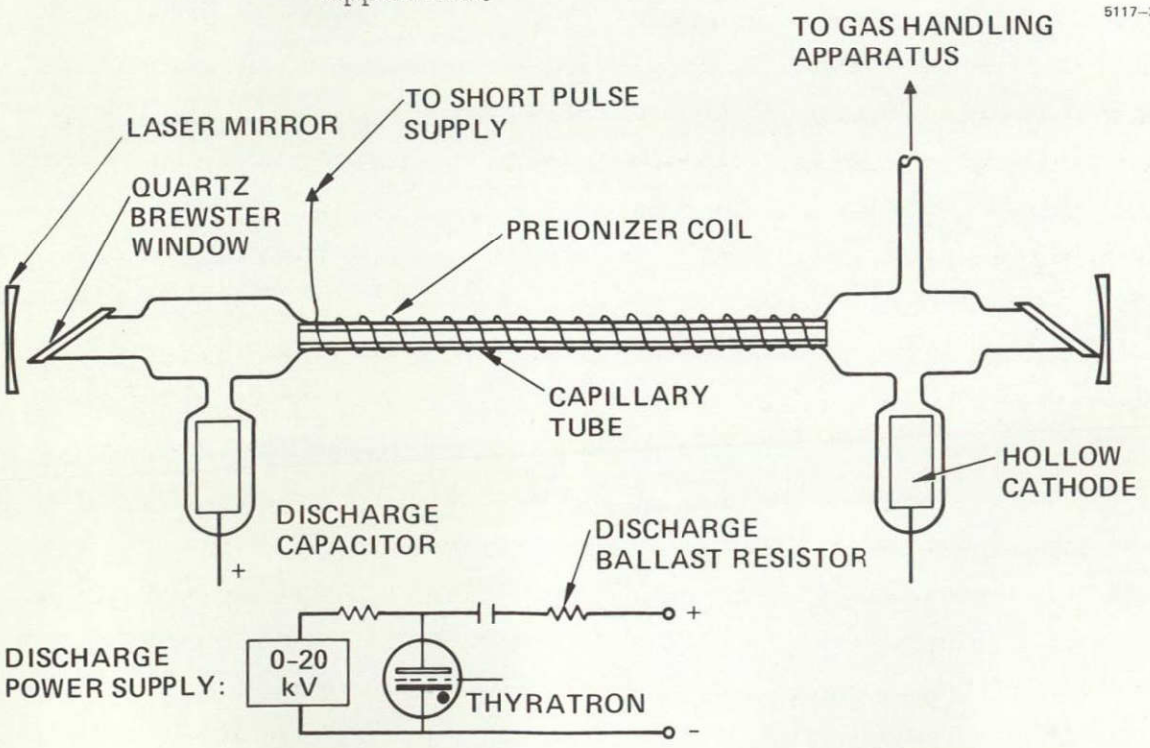

Figure IV-2. Schematic diagram of XeF capillary discharge tube and pulse circuit.

We have also designed and constructed an apparatus for conducting discharge experiments with potassium-rare gas mixtures at temperatures between 250 to 300°C. A schematic drawing of the high temperature apparatus is shown in Figure IV-3. Separate ovens are used for the discharge tube and potassium reservoir in order to eliminate condensation effects in the discharge tube. Homgeneous mixtures of potassium vapor and rare gases are prepared in a 100 cm^3 stainless steel cylinder. Partial pressures of potassium are controlled by the temperature of this reservoir which contains enough potassium to produce satuated vapor pressures. The small volume discharge tube is then filled by gas expansion from this chamber; the precise potassium dimer (K_2) absorption at 6328 Å and resonance line absorption by atomic potassium at 7665 Å and 7699 Å. A photograph of this apparatus is shown in Figure IV-4. The remainder of the electrical and gas handling apparatus for the potassium experiments is shown in Figure IV-1.

All of the discharge experiments conducted on this program have been done with the apparatus shown in Figures IV-1 and IV-2 and will be discussed in the following section. Absolute fluorescence measurements were conducted with a variety of gas mixtures and electrical parameters in order to evaluate discharge characteristics and laser potentialities. The optical configuration used for this purpose is shown schematically in Figure IV-5. A calibrated photodetector and optical filter were used to measure the side light emission from a well-defined volume in the discharge tube. These measurements can then be used to determine excited state populations of XeF and the maximum optical gain coefficient, α, with the assumption that the lower laser level is unoccupied. The relationships used to obtain this information are given below.

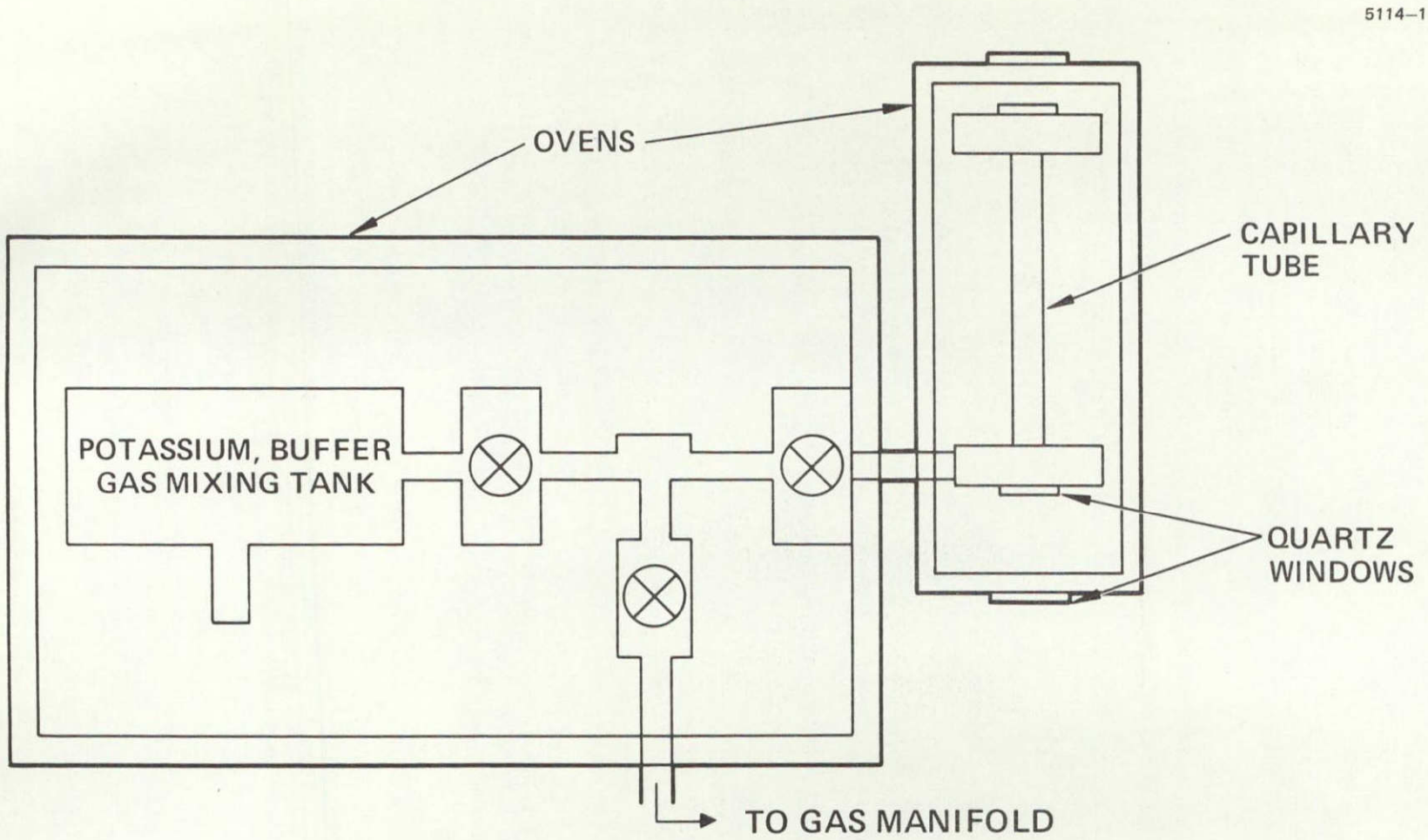

Figure IV-3. Schematic diagram of potassium rare gas discharge apparatus.

M11553

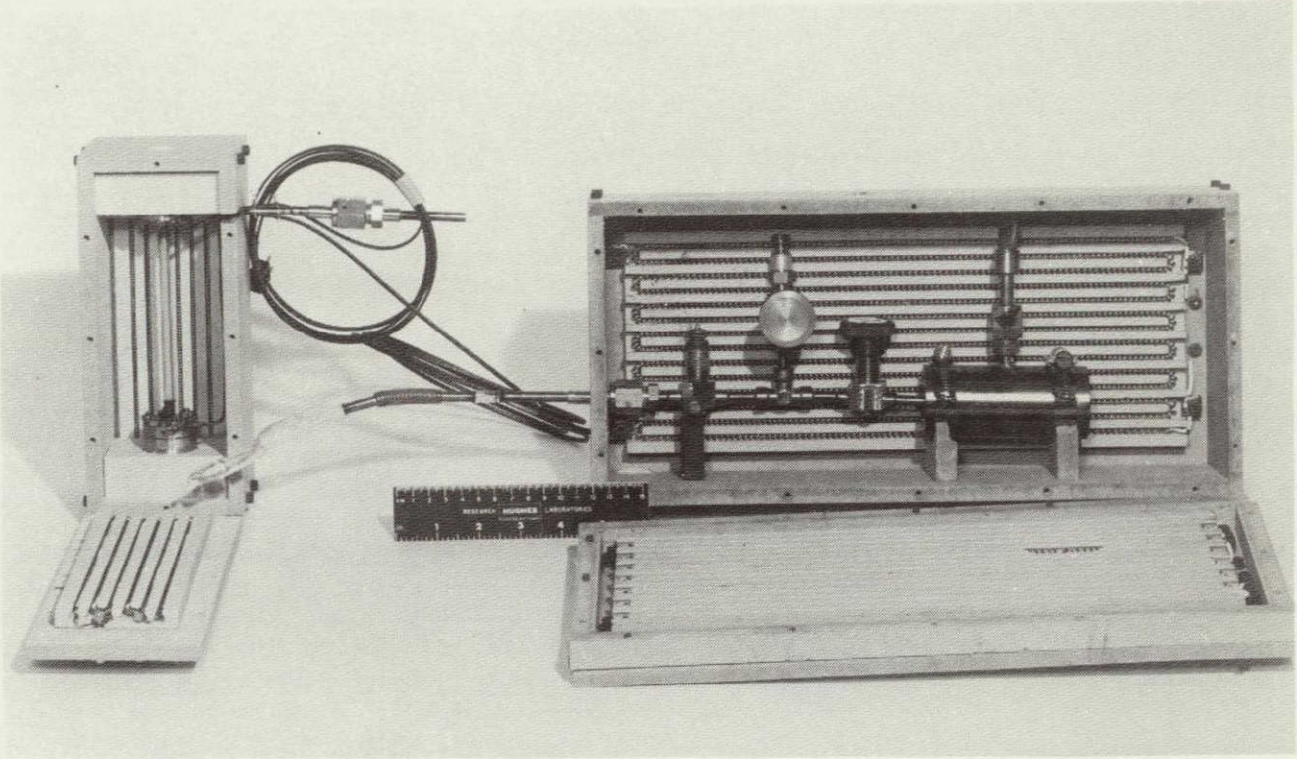

Figure IV-4. Photograph of potassium rare gas apparatus in final stages of fabrication.

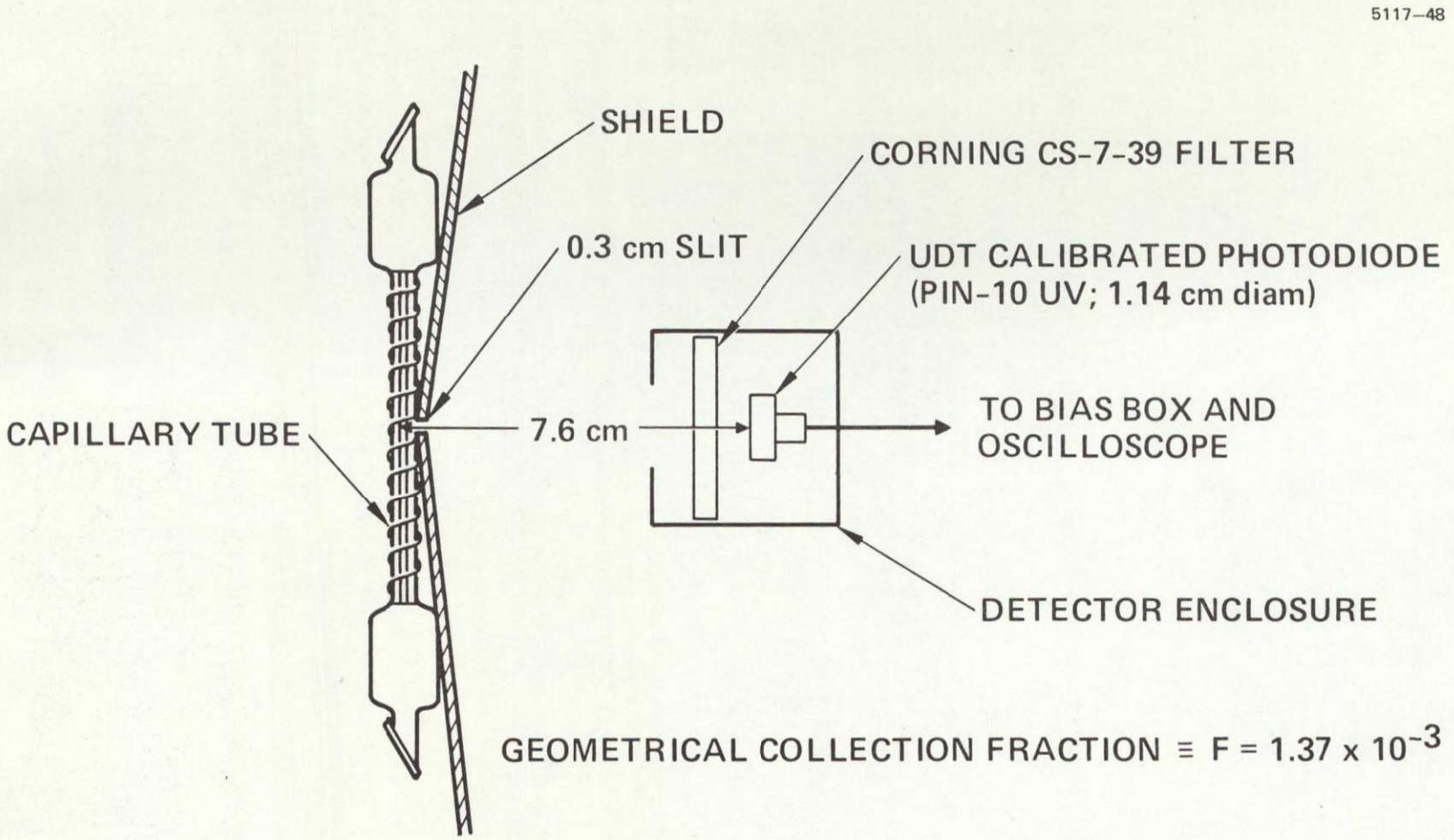

Figure IV-5. Experimental arrangement for absolute fluorescence measurements.

$$P_T = \frac{S_D}{FT} I_D$$

$$(XeF^*) = \frac{\lambda}{hcA} \left(\frac{P_T}{V}\right)$$

$$= \frac{\lambda_o^4 A}{4\pi^2 c \Delta\lambda} (XeF^*)$$

where

P_T = total optical power emitted from volume, V

I_D = photodetector current

F = geomtrical collection fraction (1.37×10^{-3})

S_D = detector sensitivity (10 W/A at 3450 Å)

T = average transmission of filter (0.464 from 340 Å to 3500 Å)

A = Einstein spontaneous emission coefficient (2.0×10^7 sec^{-1})

$\Delta\lambda$ = full width at half maximum of XeF^* emission band (105 Å).

Use of the appropriate constants with the expression above shows that an upper state XeF concentration of 3.76×10^{13} cm^{-3} is required to give a small signal peak gain coefficient of 1×10^{-3} cm^{-1}.

Spectral emission profiles were measured with a 1/4 m monochromator equipped with an optical multichannel analyzer detection system. The fluorescence spectrum of XeF obtained with this apparatus is shown in Figure IV-6. An NF_3:Xe:Ar = 1:1:10 mixture at a total pressure of 30 Torr was used in the quartz capillary discharge tube to obtain these data.

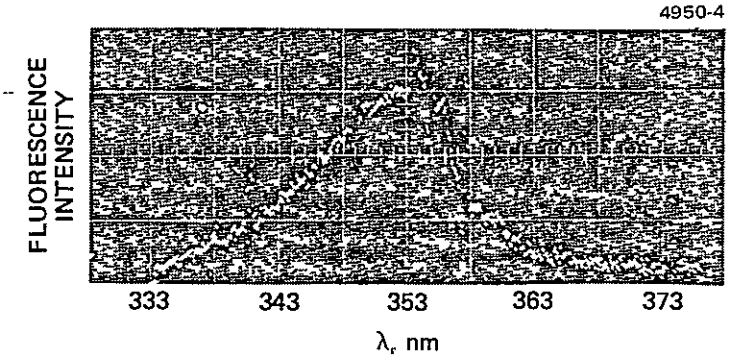

Figure IV-6. Spectral profile of XeF excimer fluorescence from capillary discharge tube.

V. EXPERIMENTAL RESULTS

A Introduction

This section contains the results of Task IV — Molecular System Evaluation. The objective of this task is to experimentally evaluate the two excimer systems recommended in Task II (K_2/KXe and XeF) with the apparatus designed under Task III (see Section IV). We describe measurements taken on the XeF capillary discharge apparatus. Operation of the K_2/KXe metal vapor capillary was delayed because of leak problems and no data have yet been obtained. It is anticipated that the metal vapor experiment will be operational early in the next contract period.

The primary measurements carried out were tests for gain and laser action, the determination of operating conditions, limiting processes, and scaling information. These latter two points are discussed in Section III. Since laser action was not achieved on XeF, additional tests were made to determine why it did not perform as predicted, with the objective of gaining new knowledge of the XeF system in order to improve the analysis of Task II (Section III).

Data obtained from the XeF apparatus included discharge voltage, discharge current, and absolute fluorescence intensity measured as a function of gas mixture, pressure, and external circuit parameters (e.g., capacitor and ballast resistor size). Upper state XeF^* populations and small signal gain were calculated from the fluorescence data according to the procedures outlined in Section IV.

Experiments were performed with two different size capillaries: (1) a 15 cm long x 0.3 cm diameter tube, and (2) a 1.6 cm long by 0.1 cm diameter tube. Tube 1 was used in the initial experiments and was designed to provide a gain path long enough for laser action and a bore size large enough to permit easy mirror alignment. Tube 2 was used in the second phase of the experiment primarily to obtain a better understanding of the system kinetics. This tube was designed to provide more efficient gas cooling and higher E/P than tube 1.

Several unsuccessful attempts at pulsed laser action were made with Tube 1 under conditions where the fluorescence measurements indicated peak gains of 8×10^{-3} cm^{-1}. The modeling studies indicated that the gas temperature was too high and E/P too low to produce an inversion. The high fluorescence yields observed were apparently dominated by thermal excitation.

Tube 2 was then used to obtain additional data under more favorable operating conditions (lower temperature, higher E/P) which were then used as input to the modeling study. The pulsed and cw performance of Tube 2 was not significantly better than Tube 1. Pulsed gains were typically 0.8×10^{-3} cm^{-1} for ~2 μsec durations. Continuous wave gains were typically 1×10^{-5} cm^{-1} and limited in duration only by the thyratron turnoff characteristics and fluorine consumption as discussed in Section III.

B. Experiments With Tube 1

The initial experiments with Tube 1, the 15 cm long x 0.3 cm i.d. tube, were carried out with a 50 to 200 kΩ resistor in series with the discharge capacitor to investigate the quasi-cw behavior of the system. Later experiments were performed with R = 0 to examine the short pulse behavior. A summary of the experimental conditions and main results of these studies is shown in Table V-1.

1. Quasi-CW Experiments With Tube 1

Both He and Ar were tried as diluents and NF_3 was employed as the fluorine source. The He mixtures typically exhibited slightly better (~20%) fluorescence intensities than comparable Ar mixtures. A typical mixture ratio used in these experiments was 1:1:2/ NF_3-Xe-He. Uniform quasi-cw discharges of 100 μsec duraction could be readily obtained at total pressures 10 Torr, at current densities of 1 to 10 A/cm^2 and E/P values of ~100 V/cm Torr. At pressures higher than ~10 Torr, the discharge would detach from the capillary wall and run a twisting course through the tube. The fluorescence intensity would be decreased by a factor of ~2 when in this mode.

Table V-1. Operating Conditions and Main Results of 15 cm Long x 0.3 cm i.d. Tube Experiments

Mixtures	NF_3.Xe·He = 0.1 – 1 5: 1 – 3 1.67 – 10
	NF_3·Xe:Ar = 1 – 1.5: 1 – 3:10
	NF_3.Xe = 1: 4 – 9
Pressures	0.5 – 10 Torr
Apparatus	C = 260 and 780 pF
	R = 0 to 200 KΩ
	20 0 kV charging voltage
Long Pulse Experiments	
	XeF* of order $10^{11} - 10^{12}$ cm^{-3} ($a \sim 10^{-5}$ cm^{-1})
	Fluorescence Pulses ~ 50 + μsec long
	Current Densities J ~ 1 – 10 A cm^2
	Steady State E/P ~ 100 V/cm – Torr
Short Pulse Experiments (R–0)	
	XeF* Peak Values of 1 to 3 x 10^{14} cm^{-3}
	Apparent Gains of a = 2.6 – 8 0 x 10^{-3} cm^{-1}
	Fluorescence Pulses ~ 0.5 μsec long
	Current Pulses ~ 0 2 μsec long, J = 100 to 4000 A cm^2
	E/P Low (Unmeasured)
	Laser Action Tried With 1 to 4/NF_3 – Xe Mixture
	Attempt Unsuccessful Because of Gas Heating

T1938

Typical data appear in Figure V-1. Fluorescence intensity, total discharge current, and total anode-cathode voltage drop are shown. After 15 to 20 μsec of fluctuations, the discharge reaches a steady state operating mode at ~1 A/cm^2 and ~120 V/cm-Torr. The steady state XeF* population is ~3.8×10^{11} cm^{-3} corresponding to a gain of ~10^{-5} cm^{-1}. Gain of this magnitude are too small for laser action in Tube 1.

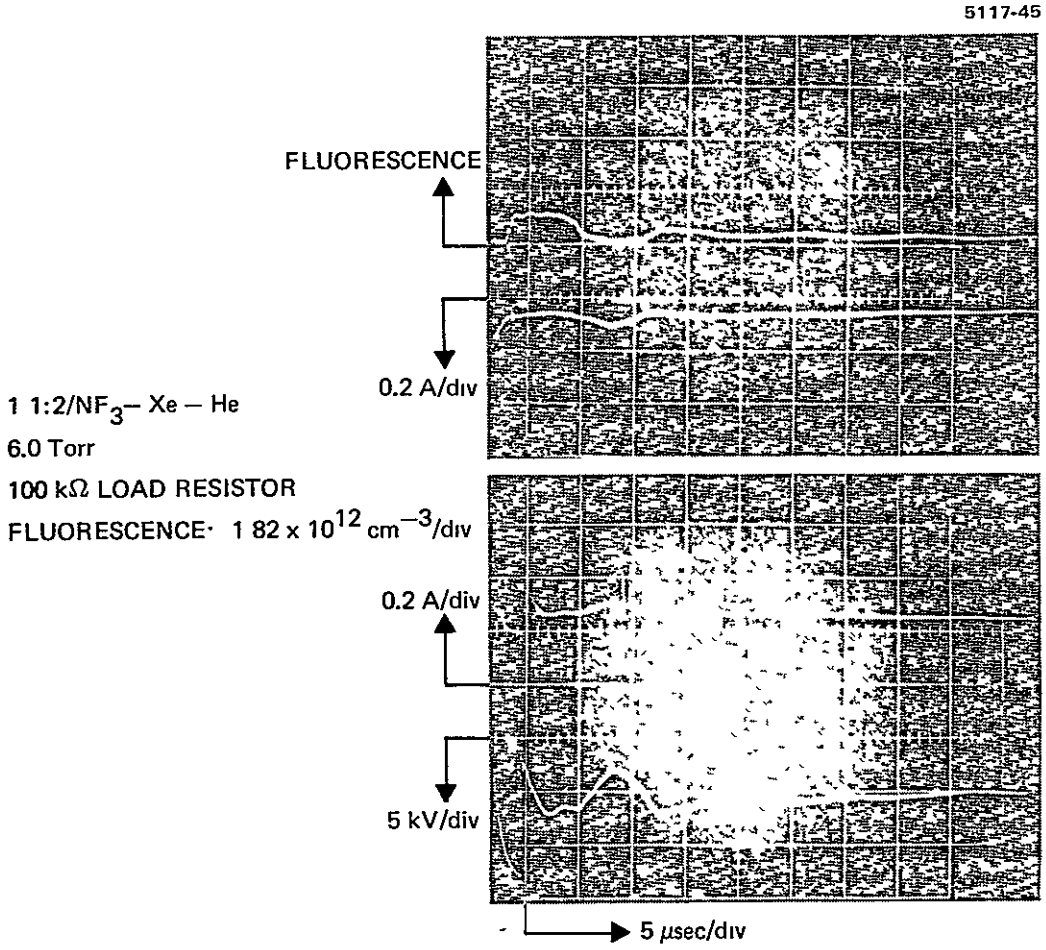

Figure V-1. Quasi-cw operation of a typical NF_3 mixture in the 3 mm tube.

2. Short Pulse Experiments with Tube 1

a. Fluorescence Optimization — As the ballast resistor (R) is decreased the current pulse shortens, the initial current rises and the fluorescence changes from a quasi-cw to a pulsed character. The peak fluorescence increases with increasing current all the way to the point where R = 0 and the current is limited primarily by the circuit inductance. The increase in fluorescence obtained by going from R = 100 or 200 kΩ to R = 0 was typically a factor of ~200.

Further increases in the fluorescence intensity were obtained by varying the mixture ratio and gas pressure. It was found that the fluorescence increased with increasing NF_3 and decreasing He diluent. Ultimately, conditions were found where peak XeF^* populations of 3×10^{14} cm^{-3} and gains of 8×10^{-3} cm^{-1} were observed. This corresponds to a single pass gain of 12% in our 15 cm tube.

Figure V-2 shows fluorescence and current traces for this maximum gain condition in the 3 mm tube. The fluorescence from this 1:4/NF_3-Xe mixture at 7 Torr has an FWHM of ~300 nsec. The current pulse is also ~300 nsec wide and reaches a peak value of ~700 A/cm^2. The discharge voltage was unmeasurable because of noise, but the E/P was probably 50 V/cm-Torr. In Figure V-2 the fluorescence trace is displaced 2 divisions to the right relative to the current trace.

b. Laser Action Experiments — Laser action was attempted with this 1:4/NF_3-Xe mixture at pressures of 1 to 10 Torr. The optical cavity consisted of two 50 cm radius mirrors spaced 40 cm apart. The mirrors were made of quartz and coated with multilayer dielectric films to give high reflectivity and 0.1% transmission near 3500 Å. This stable cavity was carefully aligned with an external He-Ne beam. A photomultiplier equipped with a narrow band 3500 Å filter was placed ~40 cm from the output window in the output beam path. The apparatus was carefully apertured so that the phototube saw only the light emitted through the output mirror. The detector system was sensitive enough to easily see the nonlasing XeF^* spontaneous emission obtained when the rear laser mirror was blocked.

5117-44

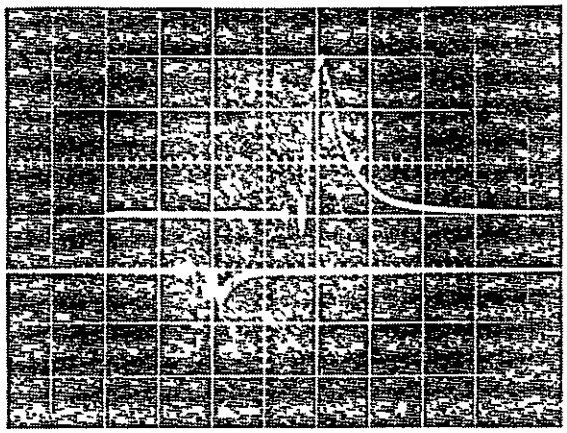

$1 - 4/NF_3 - Xe$ 7.0 Torr

780 pF AT 20 kV

NO DISCHARGE RESISTOR

TIME 0.5 μsec/div

FLUORESCENCE (TOP) 1.03×10^{14} XeF* cm^{-3}/div

$XeF^*_{PEAK} = 3.0 \times 10^{14}\ cm^{-3}$

$\alpha_{PEAK} = 8 \times 10^{-3}\ cm^{-1}$

CURRENT (BOTTOM) 100 A/div

$I_{PEAK} \cong 700\ A/cm^2$

Figure V-2. Optimized fluorescence for 3 mm tube experiments.

The onset of laser action with the above system would have been observable as a drastic (several orders of magnitude) change in the photomultiplier signal level. By comparing the detector signals obtained with the rear laser mirror blocked and unblocked, even extremely weak laseing action should have been observable.

No change in the phototube signal was observed despite pressure and current variations as well as mirror excursions performed about the He-Ne alignment condition. Laser action with a 1.5:3.0: $10/NF_3$-Xe-He mixtures was also tried with a similar lack of success.

As was explained in Section III, the lack of laser action is probably due to a high gas temperature and low E/P brought on by the high current densities required to give apparent gains of practical magnitude. The high fluorescence yield is not due to selective excitation of XeF*, but instead is the result of thermal pumping which also populates the XeF ground state.

c. Experiments With the 1.6 cm Long x 0.1 cm i.d. Tube (Tube 2) — Quasi-cw as well as short pulse operation was also examined in the 1 mm tube. Current densities were usually kept below 50 to 75 A/cm^2 to prevent significant gas heating. A summary of the experimental conditions and main results of the 1 mm tube studies are shown in Table V-2.

1. Quasi-CW Experiments With Tube 2

a. Measurements on NF_3 and F_2 Mixtures — The first experiments with the smaller tube were directed toward quasi-cw operation. Both F_2 and NF_3 were used as fluorine sources and He was used as a diluent. A typical mixture investigated was $0.2:1:1/NF_3(F_2)$-Xe-He. Data for this mixture ratio are shown in Figure V-3 (with NF_3) and Figure V-4 (with F_2). Total anode-cathode voltage drop, XeF* fluorescence intensity and total discharge current are shown as functions of total pressure. Operating pressures were usually limited to below 30 to 40 Torr by the discharge not breaking down.

The NF_3 data (Figure V-3) show that after an initial 50 to 100 μsec high fluorescence period with XeF* $\cong 1.5 \times 10^{12}$ cm^{-3}, the discharge voltage and current reach a steady state and produce a quasi-cw XeF* population for ~0.5 msec. The termination of the fluorescence is caused by the turnoff of the thyratron and is not due to kinetics effects. Rough calculations indicate that the fluorescence could remain at these levels for several milliseconds before NF_3 consumption effects become significant.

Table V-2. Operating Conditions and Main Results of 1.6 cm long x 0.1 cm i.d. Tube Experiments

Mixtures	NF_3:Xe·He = 0 1 to 1:1:1 – 2
	F_2:Xe:He = 0.2·1:1
Pressures	0.5 – 40 Torr
Apparatus	C = 260 and 780 pF
	R = 5 to 500 KΩ
	20 kV Charging Voltage
Long Pulse Experiments	
	Steady State XeF* of $2 - 4 \times 10^{11}$ cm^{-3} Observed for 0 5 msec Durations in NF_3 and F_2 Mixtures
	Steady State Gains = $0\ 5 \times 10^{-5} - 1\ 0 \times 10^{-5}$ cm^{-1}
	$J \cong 1 - 5$ A cm^2
	E/P ≅ 60 to 250 V/cm – Torr
Short Pulse Experiments (R > 5 KΩ)	
	Peak XeF* of $\sim 3 \times 10^{13}$ cm^{-3} ($\alpha \sim 0.8 \times 10^{-3}$ cm^{-1})
	Fluorescence Pulses 1 to 20 μsec Long
	$J \cong 5 - 50$ A cm^2
	Discharge Runs at High E/P (400 to 700 V/cm – Torr) for ~ 5 μsec at Start
	Discharge Then Makes Transition to Lower E/P (80 to 300 V/cm – Torr)
	Maximum Fluorescence Occurs During High E/P Initial Phase

T1939

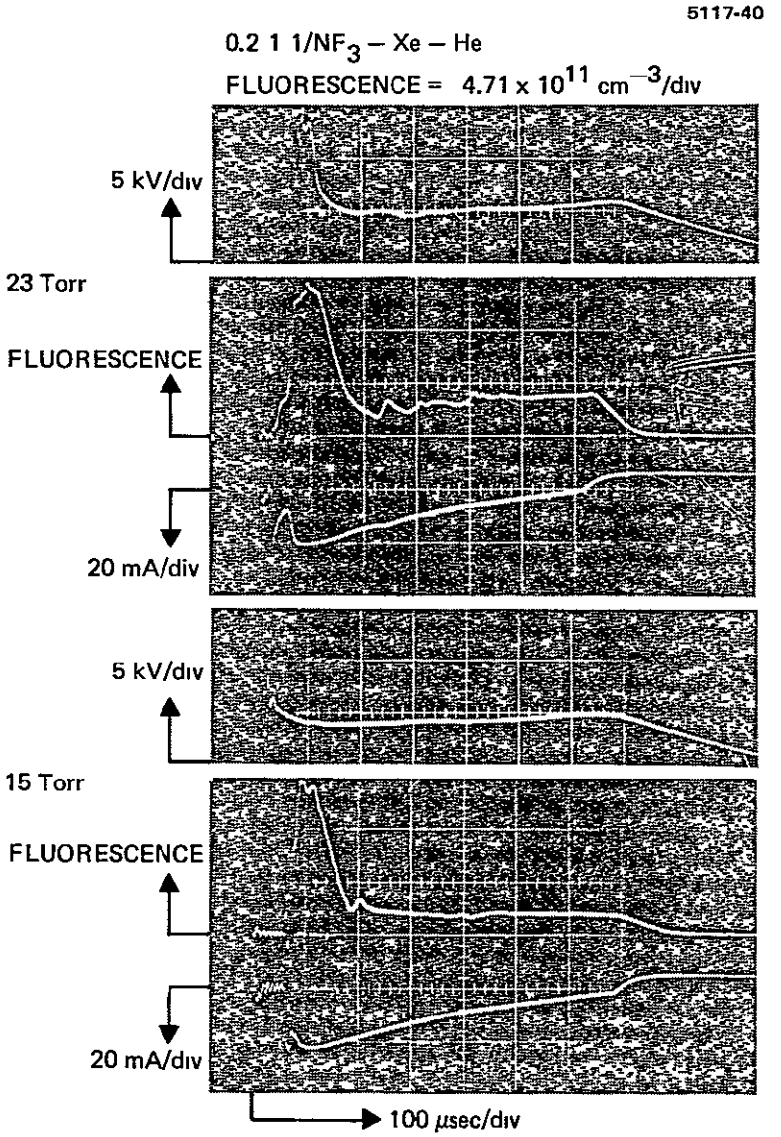

Figure V-3(a). Quasi-cw operation in typical NF_3 mixture.

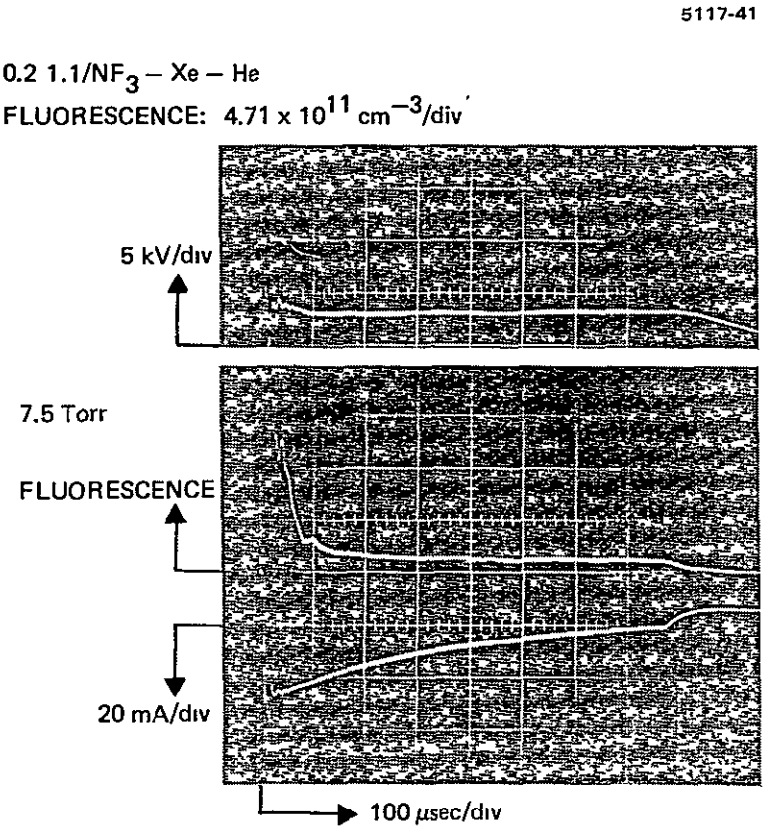

Figure V-3(b). Continued.

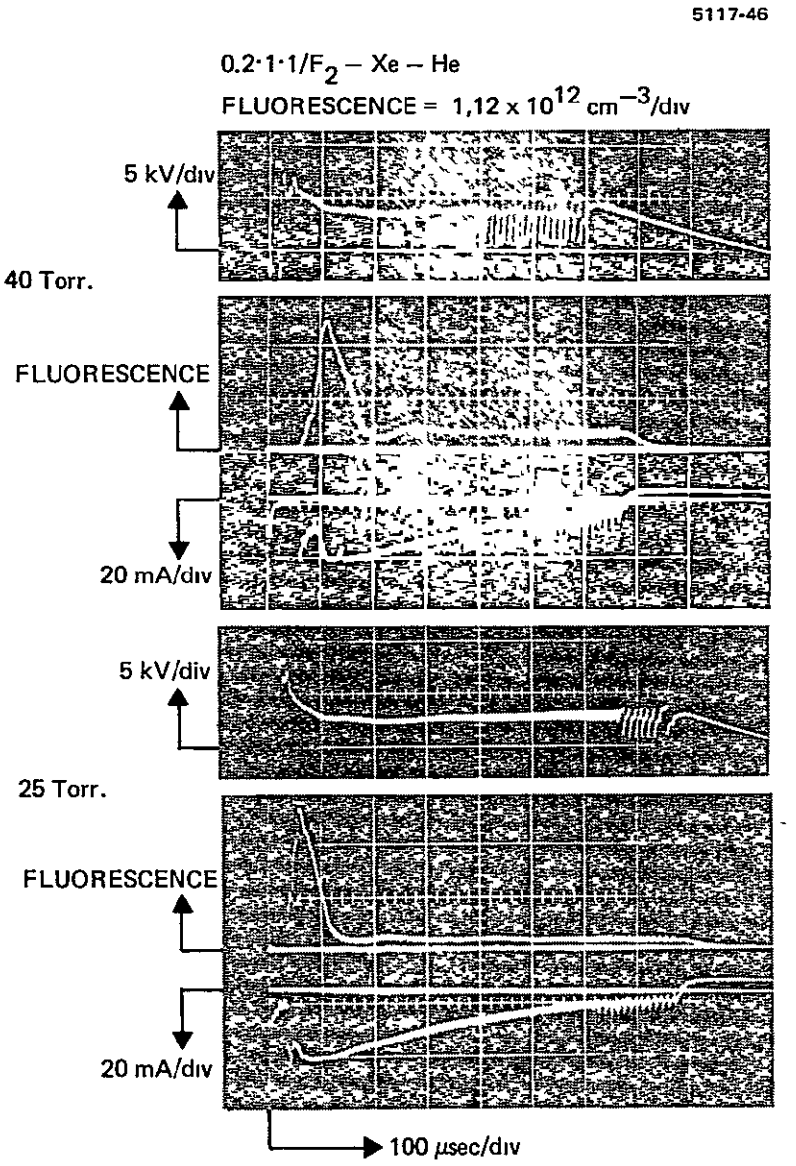

Figure V-4(a). Quasi-cw operation in typical F_2 mixture.

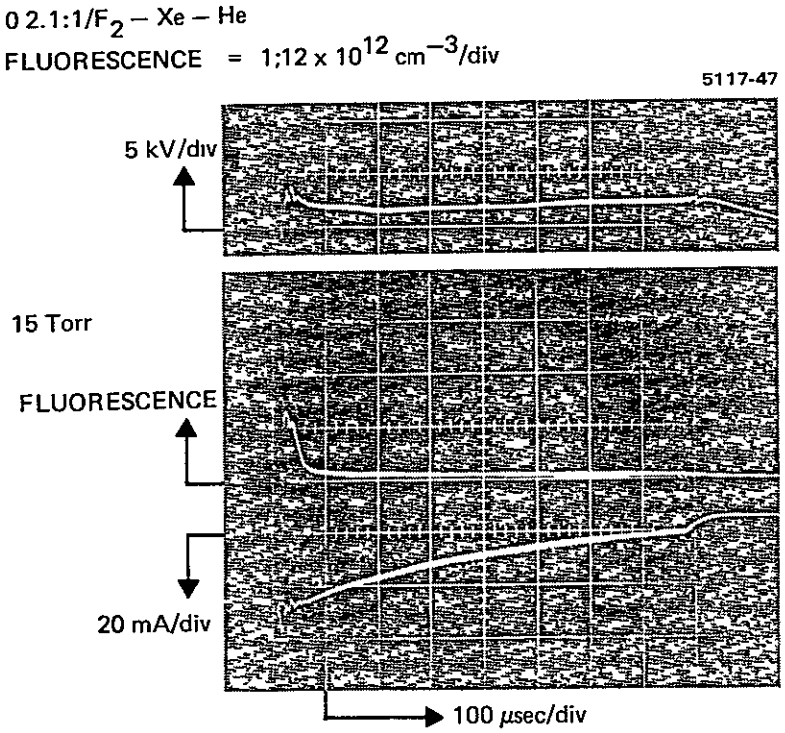

Figure V-4(b). Continued.

The steady state fluorescence scales approximately linearly as the total pressure from a value of 1.2×10^{11} cm^{-3} at 7.5 Torr to 3.7×10^{11} cm^{-3} at 23 Torr. The corresponding quasi-cw gains are 0.3×10^{-5} cm^{-1} and 1.0×10^{-5} cm^{-1}, respectively. Steady state E/P falls from 250 V/cm-Torr at 7.5 Torr to 135 V/cm-Torr at 23 Torr. Current densities are about 2 A/cm^2 for all three cases shown.

It should be noted that the current does not decay as fast as is indicated in Figure V-3. About half of the decay is caused by the 0.06%/μsec droop (36% in 600 μsec) of the Pearson 2100 Rogowski coil used in these measurements. This spurious decay is quite evident at the end of the discharge where the current trace is observed to undershoot the baseline.

The F_2 data (Figure V-4) show similar time and pressure variations. After an initial transient, a 0.5 to 0.7 msec quasi-cw fluorescence level is observed during a period of nearly constant discharge current and voltage. The steady state fluorescence again scales approximately linearly with pressure from 1×10^{11} cm^{-3} at 15 Torr (0.27×10^{-5} cm^{-1} gain) up to 4.5×10^{11} cm^{-3} at 40 Torr (1.2×10^{-5} cm^{-1} gain). The mixtures containing F_2 thus produce about one-half as much fluorescence as corresponding ones containing NF_3. This may be a result of the visually poorer discharge uniformity obtained with the F_2 mixtures. Whereas the NF_3 mixtures were uniform across the entire tube bore, the F_2 mixtures were noticeably brighter at the tube center than they were near the tube wall. The steady state E/P was also lower in the F_2 mixtures, decreasing from 80 V/cm-Torr at 15 Torr to 60 V/cm-Torr at 40 Torr.

b. Fluorine Atom Recombination Experiment — As discussed in Section III, a significant factor limiting cw operation is consumption of the fluorine source by the reaction $Xe^* + F_2(NF_3) \rightarrow XeF^* + F(NF_2)$. One way to circumvent this problem is to add a large amount of diluent to the mixture to enhance the three body recombination reaction $F + F + He \rightarrow F_2 + He$. To see if this recombination reaction would have any effect upon the fluorescence level observed during quasi-cw operation, a $0.2{:}1{:}40/F_2$-Xe-He mixture was studied at

pressures up to 200 Torr. A 0.2:1:40 mixture at 200 Torr has the same F_2 and Xe concentrations as a 10.7 Torr 0.2:1:1 mixture, but 40 times more He to act as a third body.

Figure V-5 shows the 200 Torr operation of this mixture. The gas broke down easily, but the discharge was filamentary in nature with only about one-half of the bore filled with a bright discharge directly down the tube center. The nonuniformity in the case was much worse than in the previous 0.2:1:1 mixture. As before, the discharge lasted for ~0.7 msec at constant voltage and approximately constant current until the thyratron shutoff. E/P was 6.25 V/cm-Torr (258 V/cm-Torr Xe), and assuming that the current and XeF* population were uniformly distributed throughout the tube, these had values of 2.5 A/cm^2 and 2.35×10^{11} cm^{-3}, respectively.

This XeF* population is about a factor of two greater than that observed in 0.2:1:1 mixtures at 10 to 15 Torr, indicating that the added He may be having a positive effect. However, the filamentary nature of the discharge makes these results suspect. The "filament" could be an "arc" with a high current density and a thermally excited population, similar to the high current experiments with the 3 mm tube. Further studies are required before a definite conclusion can be made on the efficacy of the recombination approach.

2. Short Pulse Experiments With Tube 2

a. Current Density Limitations — As the current is increased in the 1 mm tube (Tube 2), the initial fluorescence intensity also increases. The current cannot be increased indefinitely, however, since eventually gas heating becomes excessive and any hope of obtaining a XeF inversion is destroyed by a lowered E/P and thermal filling of the XeF ground state. We therefore conducted several experiments in an effort to determine an upper limit on the current density below which high E/P and good XeF* fluorescence could be obtained simultaneously. This limit is found to be ~50 to 75 A/cm^2 for the mixtures studied.

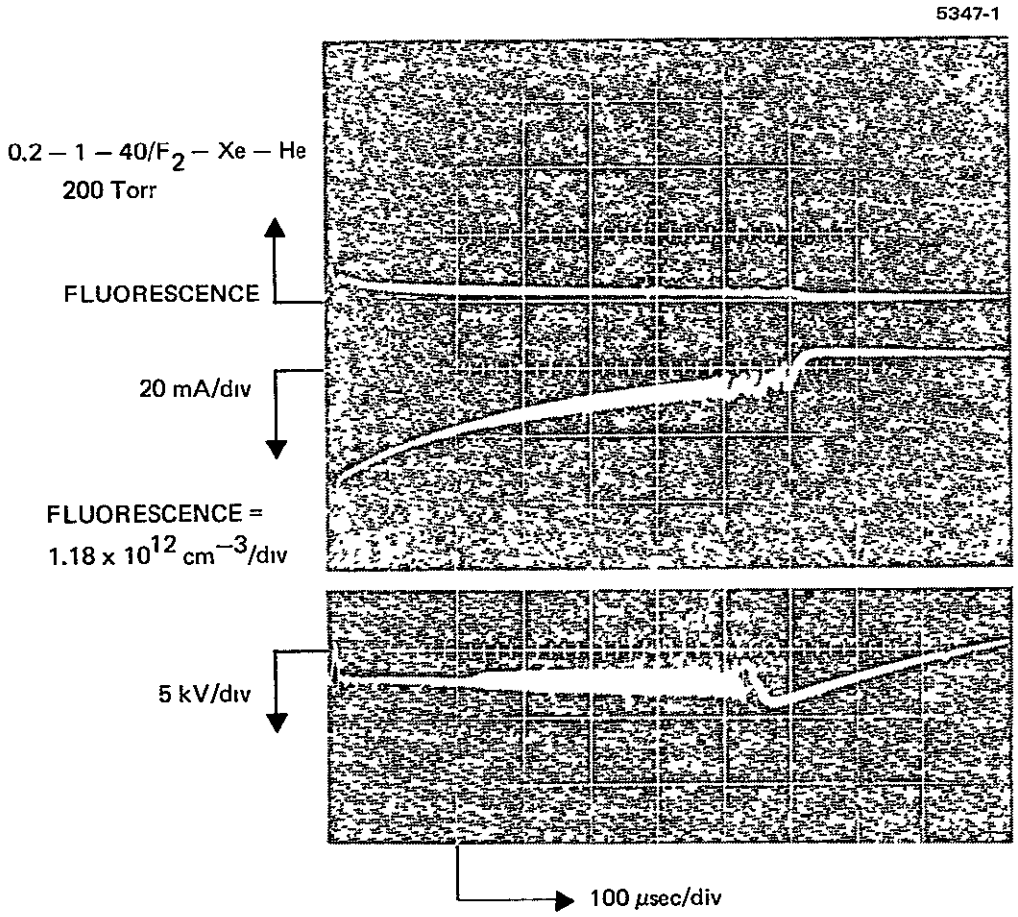

Figure V-5. Operation at 200 Torr with high helium concentration.

At current densities below this limit, high E/P is observed for ~5 μsec at the beginning of the current pulse. After this initial high E/P phase, the discharge then makes a transition to lower E/P and continues to operate there until the thyratron shuts off. The high E/P phase is characterized by E/Ps in the range 400 to 700 V/cm-Torr, while 80 to 300 V/cm-Torr is typically observed during the low E/P phase. The maximum XeF* fluorescence is observed during the low E/P phase. The maximum XeF* fluorescence is observed during the high E/P phase. The exact values of E/P obtained depend upon mixture ratio and pressure. E/P generally increases with decreasing pressure and increasing $NF_3(F_2)$.

This dual mode of operation is illustrated by photographs 1, 2, and 3 of Figure V-6. This figure shows discharge voltage and current for decreasing values of ballast resistor. An initial ~5 μsec voltage hump (the high E/P phase) is followed by a relatively flat voltage trace (the low E/P phase). Despite the fact that the current density varies from ~10 A/cm^2 in photograph 1 to ~40 A/cm^2 in photograph 3, all three cases exhibit E/Ps of ~400 V/cm-Torr during the first phase and ~125 V/cm-Torr during the second.

This collapse of the initial high E/P is primarily a result of consumption of $NF_3(F_2)$ as discussed in Section III. Since this effect is proportional to current density, one would expect the high E/P phase to shorten drastically at high current densities. This, in fact, is observed. At current densities above 50 to 75 A/cm^2 most mixtures exhibit a high E/P phase of only several hundred nanoseconds duration. This effect is illustrated by photographs 4 and 5 of Figure V-6, where initial current densities are ~150 and ~350 A/cm^2, respectively. The E/P in these mixtures falls almost immediately to low values of ~80 V/cm-Torr. At current density of this level, excessive gas heating will also have a detrimental effect upon the XeF* inversion.

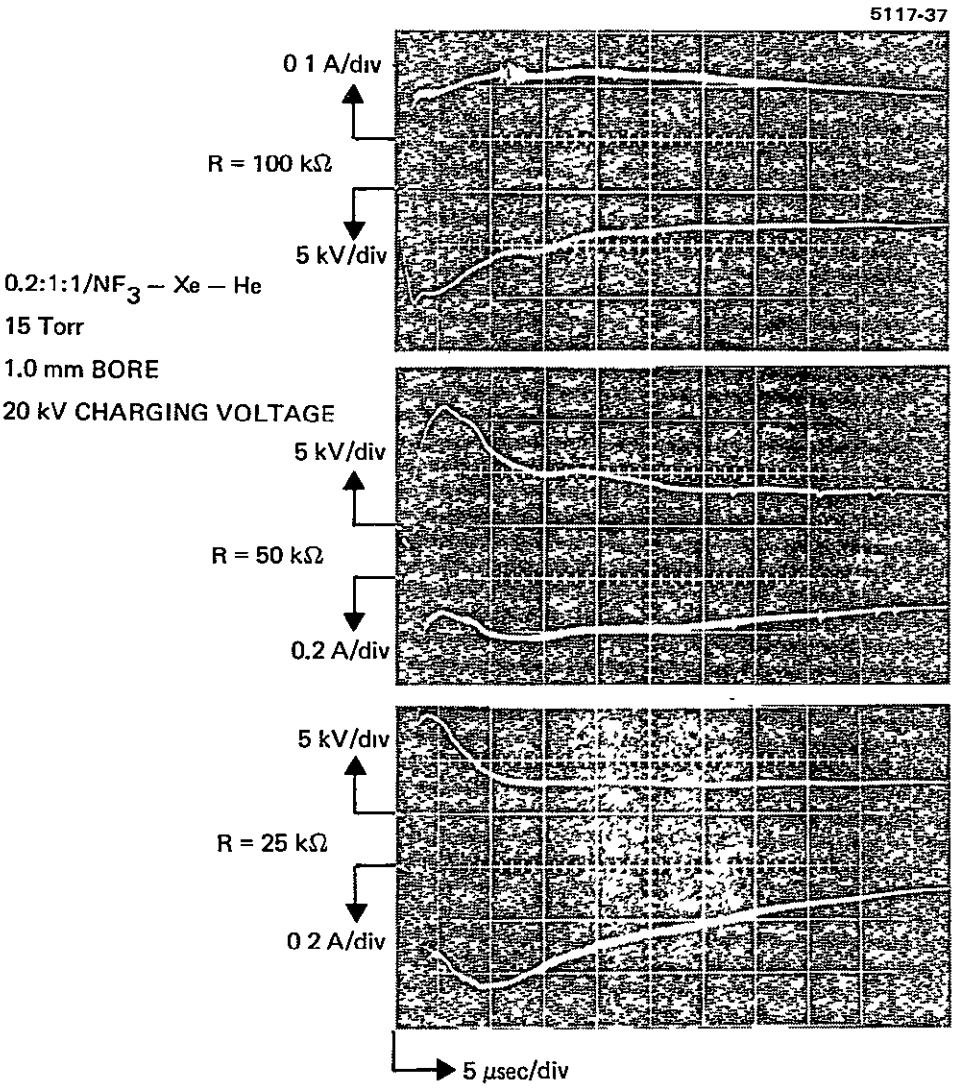

Figure V-6(a). V-I data for NF_3 mixtures illustrating current density limit.

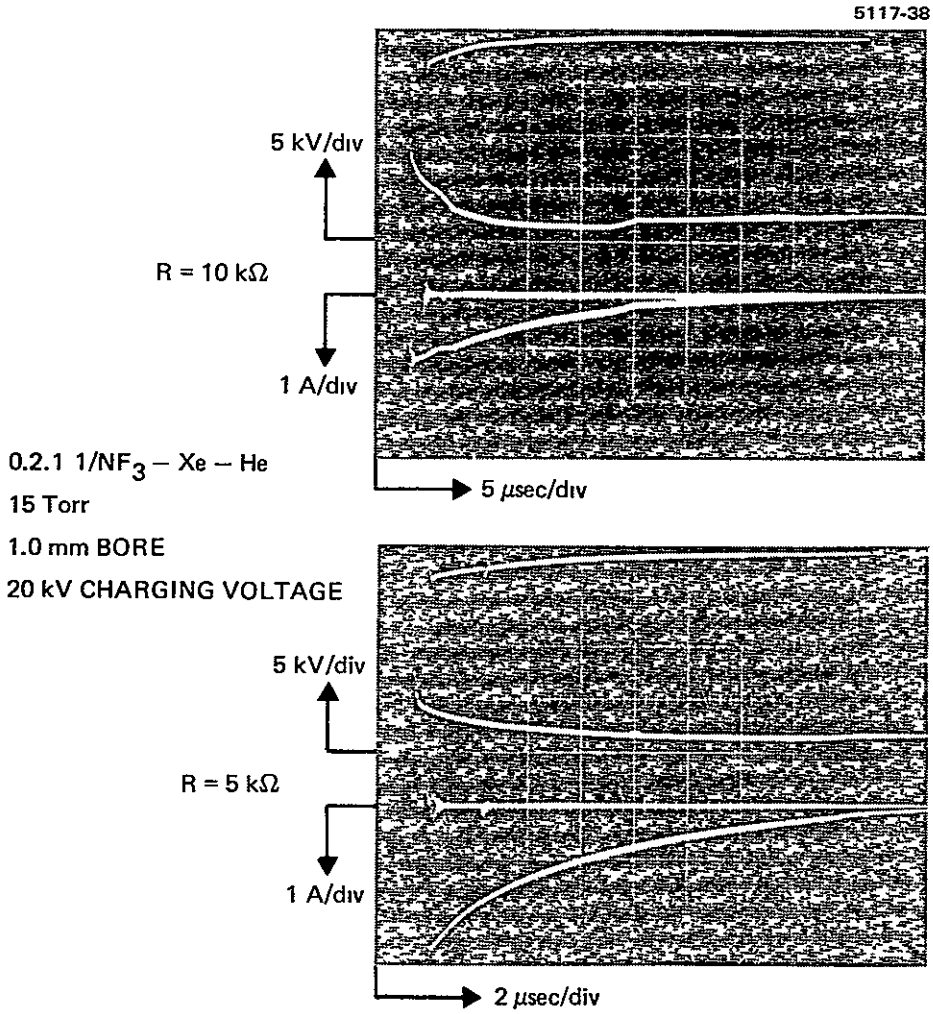

Figure V-6(b). Continued.

b. Discharge Stability — In Section III a stability condition was derived which indicated that the discharge will be stable as long as the voltage drop across the ballast resistor is greater than the voltage drop across the discharge. The data shown in Figure V-7 tend to support this stability condition.

This series of oscilloscope traces shows the V-I characteristic of a 0.2:1:1/NF_3-Xe-He mixture as a function of pressure for a fixed charging voltage (20 kV) and fixed ballast resistor (50 kΩ). In photographs 1 through 3, the peak discharge voltage is well over half of the total 20 kV on the discharge capacitor. It is 15 kV, 13 kV, and 11 kV in photographs 1, 2, and 3, respectively. The ballast resistor thus has ~5 kV, ~7 kV, and ~9 kV across it in the corresponding cases. The discharge should be unstable, and indeed the discharge current does exhibit a factor of 2 type fluctuations in the first 10 μsec of each trace.

In photographs 4 and 5, however, these fluctuations are absent. In these cases the peak discharge voltages are 8 kV and 5 kV corresponding to ballast resistor voltage drops of ~12 kV and ~15 kV. These voltages satisfy the stability criterion and indeed the V-I characteristics of 4 and 5 do come to a steady state more rapidly with less severe fluctuations than do cases 1, 2, and 3.

c. Fluorescence Measurements — With the 50 to 75 A/cm^2 limit in mind, variations in system parameters were carried out in order to maximize the XeF* fluorescence. The XeF* population was found to be a weak function of current density, pressure, and mixture ratio. Typically, the peak fluorescence would vary by only factors of 2 to 4 for fairly large excursions in operating conditions. The use of F_2 in place of NF_3 also produced only small differences in performance.

Figure V-8 illustrates how the XeF* fluorescence varies with pressure for a typical NF_3-Xe-He mixture. The optimum pressure for this mixture is ~10 Torr where XeF* ≅ 3.3×10^{13} cm^{-3} (i.e., gain ≅ 0.9×10^{-3} cm^{-1}) is obtained. The fluorescence, which is significant only during the initial part of the current pulse (high E/P phase),

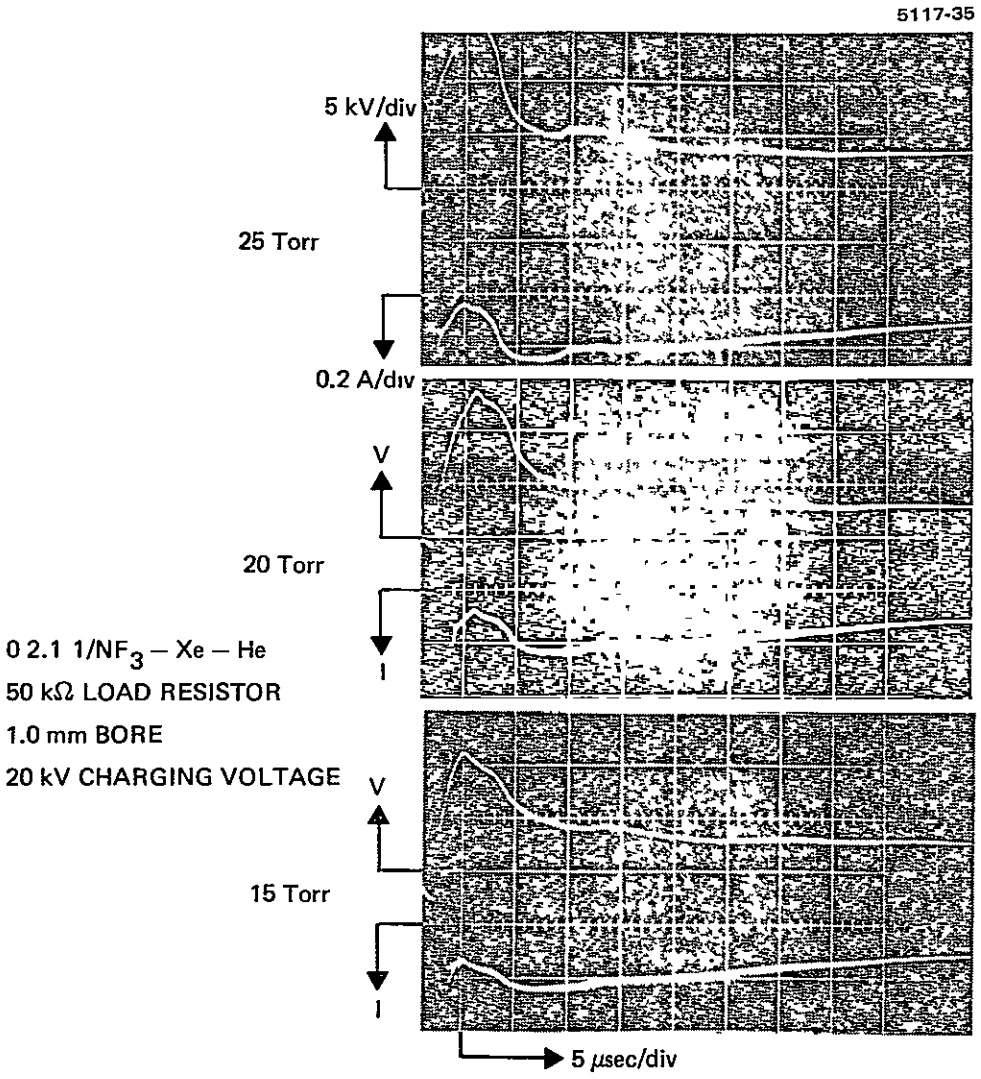

Figure V-7(a). V-I data for NF_3 mixture illustrating the discharge stability condition.

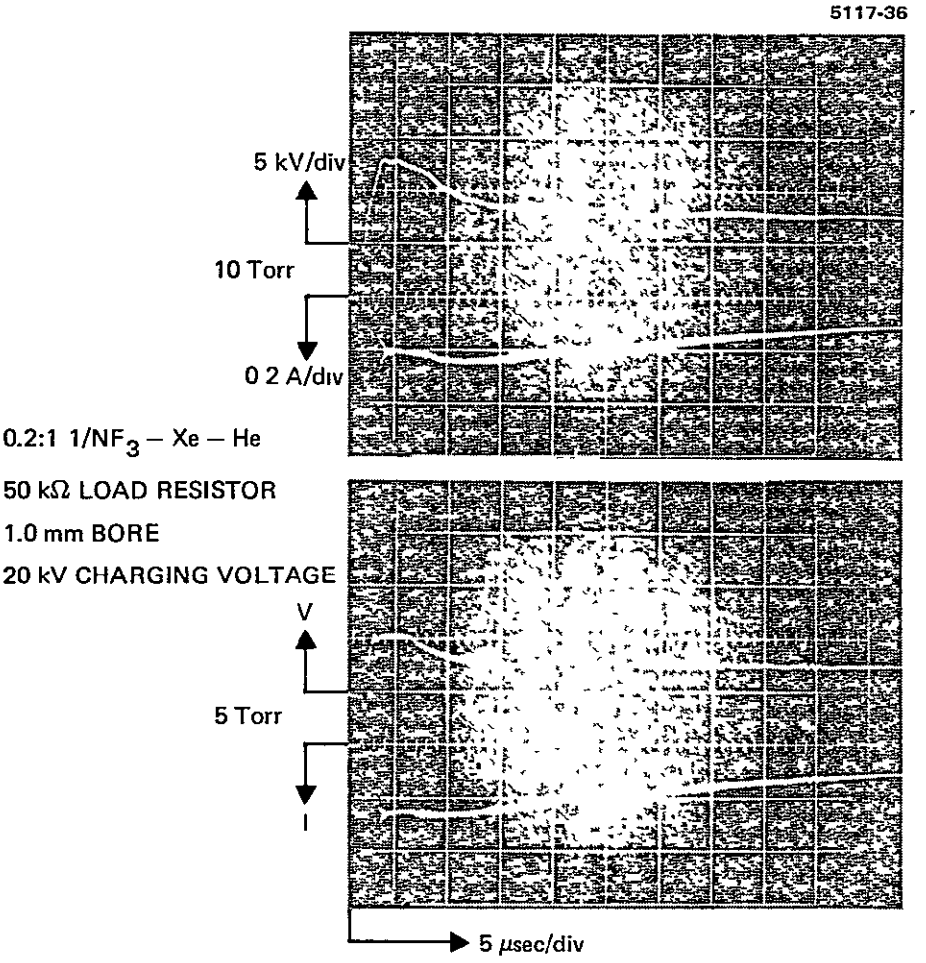

Figure V-7(b). Continued.

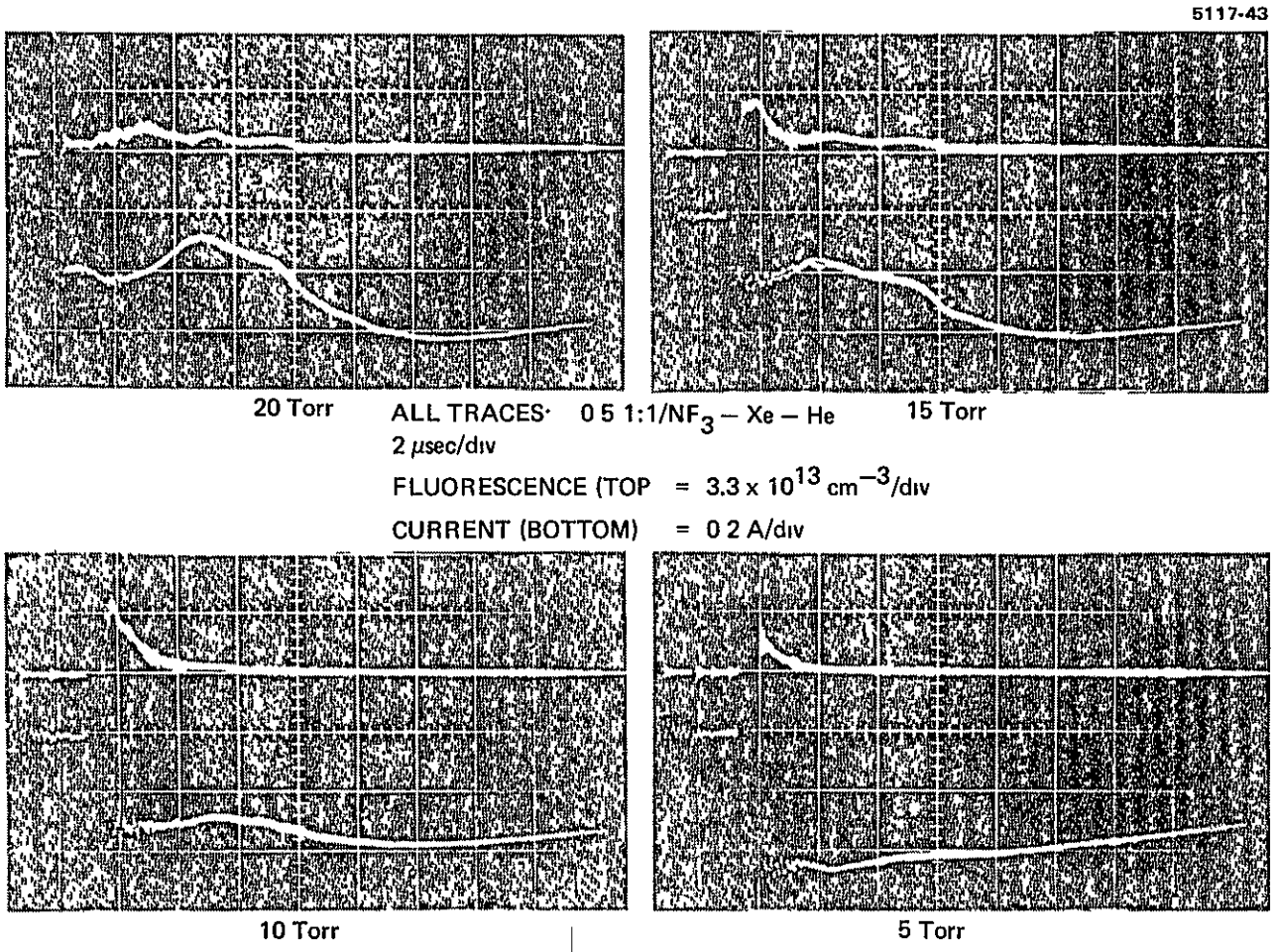

Figure V-8. Pressure dependence of fluorescence from a typical NF_3 mixture.

varies by only about a factor of two over the range 5 to 20 Torr. The current density varies from ~25 A/cm^2 at 20 Torr to ~65 A/cm^2 at 5 Torr.

Figure V-9 shows oscilloscope traces of the maximum fluorescence obtained for four different X:1:1/NF_3-Xe-He mixtures with X = 0.2, 0.35, 0.5, and 1.0. These mixtures produced the highest fluorescence of any evaluated during this part of the study. In this series, the operating pressure has been varied with constant charging voltage (20 kV) and a fixed ballast resistor (25 kΩ) until maximum fluorescence was obtained for each mixture.

Despite the wide variation in NF_3 concentration, the optimum fluorescence obtained is very nearly the same for all mixtures: XeF* $\cong 3 \times 10^{13}$ corresponding to ~0.8×10^{-3} cm^{-1} gain. As indicated previously, this lack of a strong dependence upon operating conditions appears to be a general characteristic of the XeF* capillary system and is not restricted to this particular set of mixtures.

Figure V-10 shows typical short pulse operation with F_2 at two different current levels 15 A/cm^2 (top) and 30 A/cm^2 (bottom). Despite these relatively modest current densities, the discharge does not exhibit the initial high E/P phase observed in NF_3 discharges. Maximum E/P in this mixture is ~200 V/cm-Torr. The fluorescnece observed is also somewhat lower than in the NF_3 mixtures. As in the quasi-cw experiments, the F_2 mixture discharges were visibly nonuniform with the center being considerably brighter than the regions near the walls. This lack of discharge uniformity is undoubtedly linked to the relatively poor performance of these mixtures.

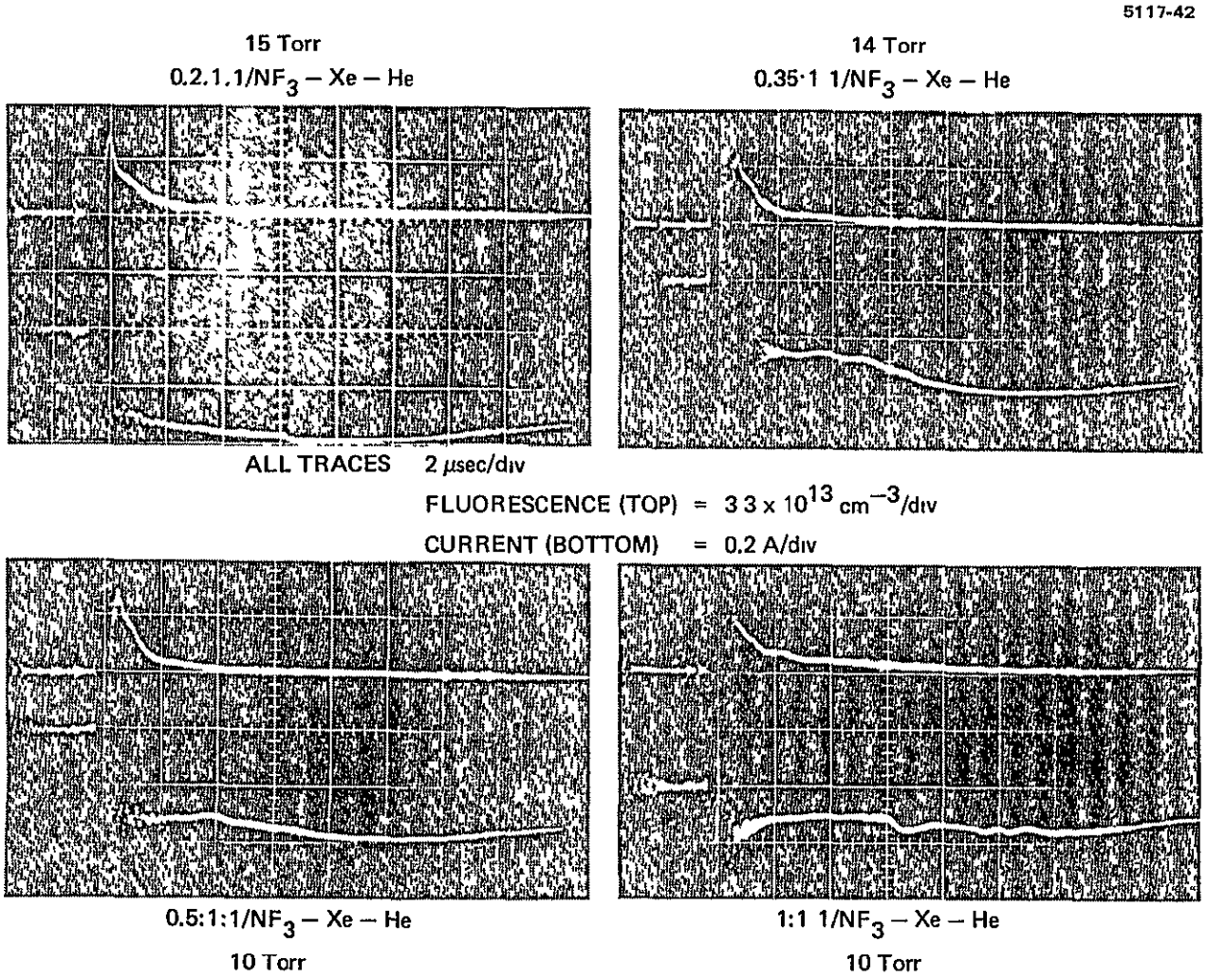

Figure V-9. Optimized fluorescence in 1 mm bore tube for several NF_3 mixtures.

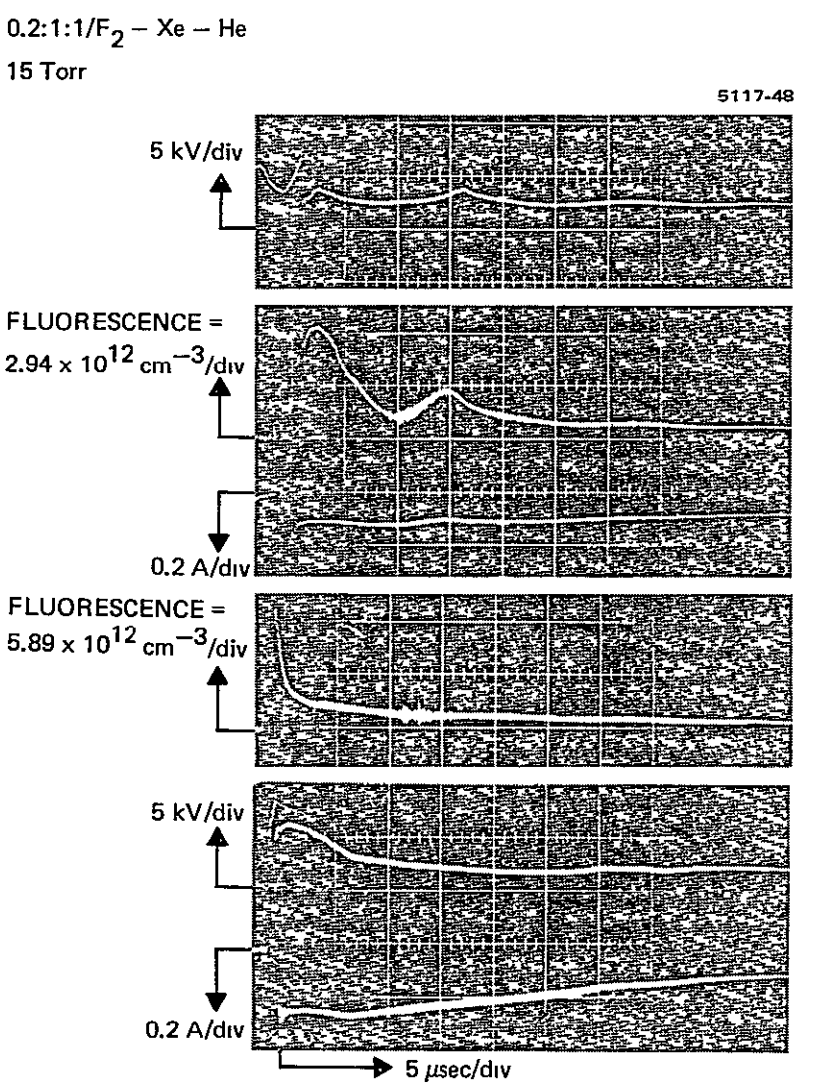

Figure V-10. Fluorescence and discharge measurements for a typical F_2 mixture.

VI. PRELIMINARY CONCLUSIONS AND FUTURE WORK PLAN

A. Preliminary Conclusions

At this point in the program we are in a position to make some preliminary conclusions regarding the expected performance characteristics of a capillary discharge pumped cw excimer laser. In both the XeF and the KXe/K_2 excimer systems the discharge electric field required for achieving a practical gain coefficient of ~1% per cm is predicted to be high, ~10 to 40 kV/cm. If the field is to be applied axially along the capillary tube it will be necessary to use multistage, individually ballasted discharge paths as shown in Figure VI-1 in order to limit the required power supply voltage to ~10 to 40 kV. This type of discharge configuration is used routinely for CO_2 waveguide lasers. The ballast resistors will need to have a voltage drop comparable to or greater than the discharge voltage on each segment so that all segments will draw equal current and run in a stable mode.

In both the XeF and KXe/K_2 excimer systems the efficiency is predicted theoretically to be near the quantum efficiency (~30% for XeF and ~90% for KXe/K_2). In the case of XeF the optimized experimental efficiencies appear to be running about a factor of 10 below quantum efficiency. At lasing threshold we expect the input current density to be $\sim 10^2$ A/cm^2 for the XeF system and ~1 A/cm^2 for the KXe/K_2 system. For cw operation both systems will likely have to run at a total pressure of between 1 to 10 atm. For adequate gas temperature cooling the capillary diameter will be required to be ~1 to 3 mm (a lower figure likely applying to the higher threshold XeF system), with at least half of the gas being helium. Flowing liquid coolants, of course, will also be necessary to control the temperature of the tube wall. Assuming that an efficiency of 10% can be reached for both systems, the expected cw power output for near threshold operation should be ~10 to 100 W for the capillary discharge pumped KXe/K_2 system and ~100 to 1000 W for the capillary discharge pumped XeF system.

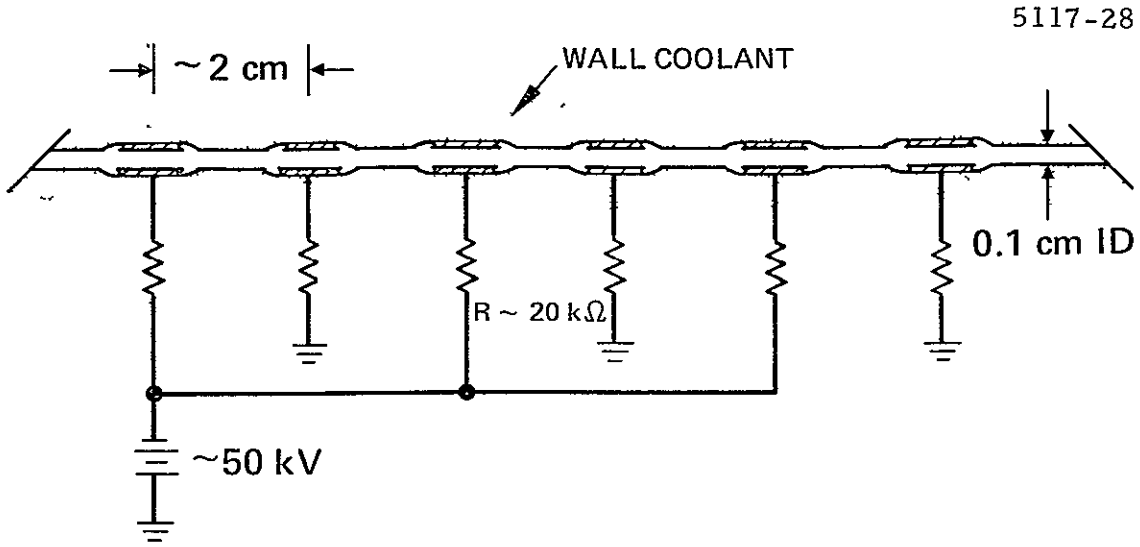

Figure VI-1. Projected capillary discharge configuration for cw excimer laser.

B. Future Work Plan

The capillary discharge technique in use for the present phase of the program was chosen as the most expedient means to demonstrate and gather basic data for cw operation of an excimer laser system. This technique is not dimensionally scalable. Thus, the appropriate goals for the future 12 month phase of the program in meeting the overall objectives of the NASA high power laser program are

1. Identify and show theoretical feasibility of a cw pumping technique which can be applied to at least one excimer system recommended from the current program and which can be scaled to produce cw output power sufficient to meet NASA's future mission requirements

2. Demonstrate feasibility of the above concept in a laboratory experiment.

According to the discussion in Section II the only option other than thermal conduction for achieving the 10^4 to 10^5 W/cm^2 heat removal rate required of a cw excimer laser is convection. For the alkali excimers this is a viable approach to more scalable cw operation since residence lengths as long as 10 cm at 1 to 10 atm pressure

sonic flow can be tolerated. In the case of the XeF system the maximum residence length required could be as short at 1 mm, which would not offer any improved scalability features over the capillary discharge. However, there is a particular feature in the XeF excimer system pumping kinetics that permits consideration of a new non-quilibrium convection and radiative cooling mechanism for achieving scalable cw operation of this system at low pressure.

In the case of the XeF excimer lasers, gas flow can be used in a unique way to permit power extraction throughout a dimension >1 cm in the flow direction. The method is to utilize a unique feature of the kinetics of these excimer systems which will permit one to use low pressure gas flow to spatially separate regions of the flow where electron-heavy particle thermalization has occurred (downstream region) from the region where the electron and gas temperature are still disparate (up-stream region). The unique feature is the fast two-body excimer formation rate, e.g.,

$$Xe^* + F_2 \rightarrow XeF + F \quad , \tag{26}$$

which at low pressures ~1 to 10 Torr can proceed rapidly enough to quickly reach lasing threshold and, in particular, proceeds at a rate faster than the electron-heavy particle thermalization rate which occurs primarily via vibration-to-translation transfer collisions. The rate for the former process is $\sim 10^{-9}$ cm^{-3} sec^{-1} while the V-T transfer rate is at least two orders of magnitude smaller.

Assume a 10:1 Xe:F_2 mixture at a density of 10^{17} cm^{-3} and flowing at a speed of $\sim 10^5$ cm/sec. Energy is fed into the electrons at the head of the plasma jet and establishes an electron temperature of ~4 eV (typical of pulsed static XeF_2 discharge pumped excimer lasers). These electrons quickly establish comparable reservoirs of electronic level energy [Xe*] $\approx 10^{14}$ cm^{-3} and vibrational level energy [F_2'] $\approx 10^{14}$ cm^{-3}. At these densities and at the above flow velocity, reaction (26) will establish an excimer level population sufficient for lasing in about 0.1 mm, i.e., at essentially the upstream boundary of the plasma jet, while V-T transfer and thermalization will not be complete

until several centimeters downstream (see Figure VI-2). In this latter region the gas will become hot (Tg ~ 1 eV) and radiative cooling can occur thus giving the added benefit of helping to minimize the heat exchanger bulk in a recirculating system.

Finally, the fluorine consumption problem associated with cw low-pressure operation of this system is removed as the gas flow is adequate to replenish the fluorine at the required rate.

In principle, the above concept is similar in many respects to many chemical lasers but differs of course in the sense that power must be put into the medium by means of a discharge. If, as anticipated, laser power extraction can occur throughout plasma jet volumes on the order of 1 cm^3, a gain path of 50 to 100 cm could provide net cw laser power levels in the range that would meet NASA's ultimate mission requirements.

Whether one uses equilibrium or nonequilibrium gas flow to establish cw operation of an excimer laser with gas residence length of 1 cm, one must in either case first demonstrate stable operation of a transverse discharge in a static gas for times ~10 μsec which roughly corresponds to the sonic flow residence time of gas in the discharge. This will be done in the forthcoming phase of the program for both the KXe/K_2 and XeF systems prior to any experiments utilizing gas flow.

In total, the activities planned for the forthcoming year are

1. Achieve spontaneous emission brightness levels adequate for lasing KXe K_2 or XeF in
   - a cw capillary discharge
   - a 10 μsec static transverse discharge

   } Parallel activities for first six months

2. Construct and achieve cw laser action in a long gain-path capillary discharge
3. Construct and achieve several millisecond laser action in a fast flow transverse discharge.

} Parallel activity for second six months

$e^- + Xe \longrightarrow Xe^* + e$

$e^- + Xe \longrightarrow Xe^+ + e$

Xe^*

$e^- + F_2 \longrightarrow F^- + F$

$Xe^* + F_2 \longrightarrow XeF^* + F$

$e + F_2 \longrightarrow e + F_2\,(VIB)$

} FAST (< 1 μsec)

$F_2\,(VIB) + Xe \longrightarrow F_2 + Xe\,(TRANS)$

$F_2 + Xe \longrightarrow XeF_g + F$

} SLOW (> 10 μsec)

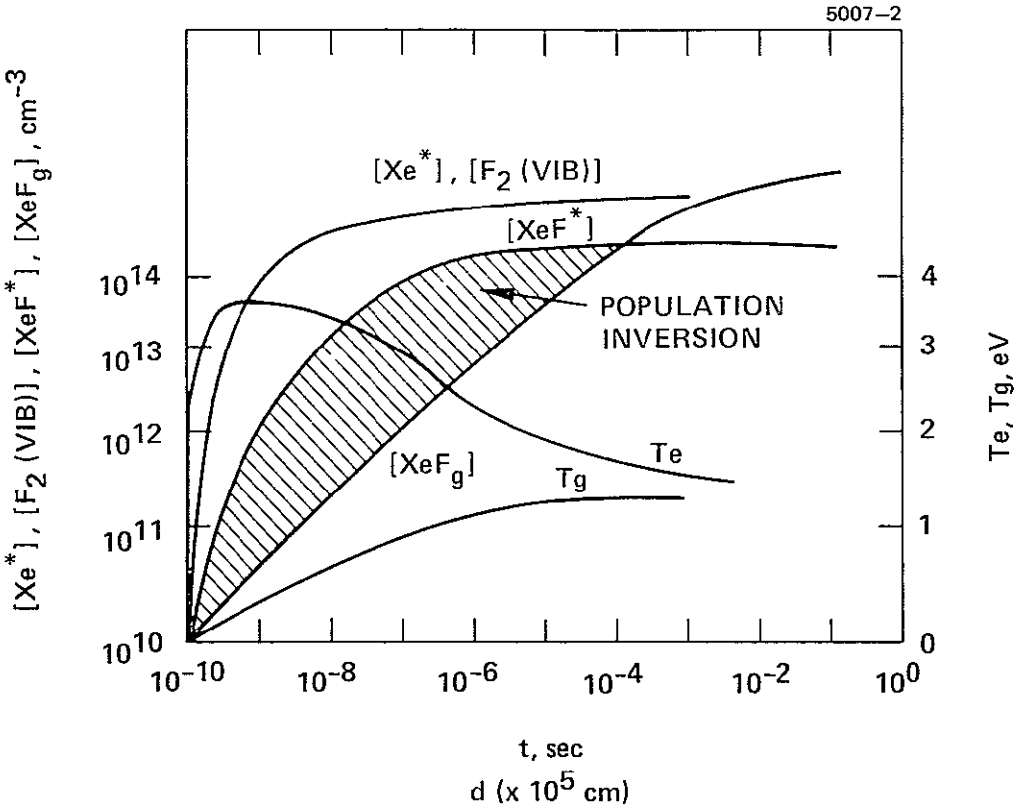

*CW OUTPUT POWER ≅ 10 MW/liter

Figure VI-2. Low pressure XeF excimer plasma jet concept.

At the end of this second year effort on the program we expect to have identified both an excimer molecular system and cw pumping technique which is dimensionally scalable to cw power levels on the order of one megawatt and to have carried out a small scale demonstration of lasing such a system in the laboratory.

REFERENCES

1. C. E. Moore, Atomic Energy Levels, National Bureau of Standards.
2. H. M. Michaels and F. E. Harris, J. Chem. Phys. 19, 1464 (1963).
3. A. J. Palmer, J. Appl. Phys. 41, 438 (1970).
4. J. Pascale and J. Vandeplanque, CEA Report, March 1974.
5. C. York and A. Gallagher, Jt. Inst. Lab. Astrophys. Rpt. 114, October 1974.
6. R. Carbone and M. Litvak, J. Appl. Phys. 39, 2413 (1968).
7. R. Hill et al., Appl. Phys. Lett.
8. C. Cooper, C. Cobb, and E. Tolnas, J. Mol. Spectrosc. 7, 223 (1961).
9. C. Herzberg, Spectra of Diatomic Molecules (B. Van Nostrand, 1950).
10. J. Ewing and C. Brau, Phys. Rev. A12, 129 (1975).
11. E. George and C. Rhodes, Appl. Phys. Lett. 23, 139 (1973).
12. A. V. Phelps, Jt. Inst. Lab. Astrophys. Rpt. 110, September 1972.
13. A. von Engle, Ionized Gases (Oxford Clarendon Press, 1965).
14. L. J. Kieffer, Jt. Inst. Lab. Astrophys. Information Center Rpt. No. 13, University of Colorado, September 30, 1973.
15. S. C. Brown, Basic Data of Plasma Physics (The MIT Press, 1967.
16. P. Mahadevan and R. Hofland, Aerospace Corporation reprint (1976).
17. C. A. Beam and J. J. Ewing, Semiannual Tech. Rpt., Contract N00014-75-C-0063, Avco Everett Research Laboratories, Inc.
18. R. E. M. Hodges, D. L. Drummond, and A. Gallagher, Phys. Rev. A6, 1519 (1973).

19. O.S. Heavens, J. Opt. Soc. Am. 51, 1058 (1961).

20. J. Holstein, Phys. Rev. 72, 1212 (1947).

21. A.J. Palmer, J. Appl. Phys. 47, 3088 (1976).

APPENDIX

Section 1

```
C XEFL - DISCHARGE PUMPED XEFL LASER
      REAL MASE,MASXE,MASM,M1,M2,MI,K,K3X,K5X,K41,NEO,NE
      REAL NEP
      REAL J
      REAL M
      REAL LENGTH
      REAL KPLUS,KNI,KEL
      REAL L
      REAL MD1,MDI,MD
      EXTERNAL FUNC
      COMMON/STOR/M,XE,NE,NEP,CM1,CX1,XEFG,EM1,EX1,EXEFU,CEL,
     +MASE,MASM,V,LENGTH,A,L,R,DT,E,FL
C CONSTANT DATA
      MASE=0.5E6; E=1.6E-19; MASXE=131*1840*.5E6
      L=0
      C=1000E-9
      D=.1
      A=3.14*(D/2)**2
C M=HELIUM
      MASM=4*1840*.5E6
      EX1=8.3; EX2=9.6; EXI=12.08
      EM1=22.; EM2=23.; EMI=24.5
      EXEFU=3.1
      CX1=.3E-16; CX2=.05E-16; CXI=.11E-16
      CX1I=5E-16; CX2I=5E-16
      CM1=.025E-17; CM2=.025E-17; CMI=.08E-17
      CM1I=5E-16; CM2I=5E-16
      CEL=5.5E-16
      CDIF=1E-15

      LENGTH=1.6
      K=1440E19
      NEO=1E10
      TGO=.03
      AX2=4E7;AM2=32E7;AXED1=4E7;AMD1=32E7;AXEF=2E7;AMX=10E7
C INITIAL CONDITIONS
      WRITE(5, 50)
   50 FORMAT(2X,1HM,5X,2HFL,5X,2HXE,5X,2HVO,5X,1HR,5X,2HDI,
     +5X,6HIPRINT,5X,4HTMAX,5X,2HVS)
      ACCEPT*,M,FL,XE,VO,R,DT,IPRINT,TMAX,VS
      TG=TGO
      V=VO
      WRITE(5, 80)
   80 FORMAT(4X,4HTIME,6X,5HVDISC,5X,1HJ,9X,2HNE,8X,3HENI,
     +7X,2HMI,8X,3HXEI)
      WRITE(5, 85)
   85 FORMAT(7X,2HFL,8X,3HXE1,7X,4HXEFU,6X,4HXEFG,6X,4HGAIN,6X,2HTG,
     +8X,2HTE)
```

```
C TIME STEP
   20 ISTEP=ISTEP+1
      T=T+DT
      IF(T-TMAX) 21,21,22
   21 CONTINUE
C CIRCUITRESPONSE
      NE=NEO+MI+XEI+MDI+XEDI+XEMI-ENI
      VO=VO-DT*J*A/C
      IF (VO-VS) 4,5,5
    5 V=VO; GO TO 6
    4 V=VS
    6 CONTINUE
      IERR=0;IND=1;EPS=0.02
      IF (ISTEP-1) 10,10,8
    8 IF (TE-.5) 9,9,10
    9 TE=.5; GO TO 2
   10 CONTINUE
      TE=SOLN(IND,FUNC,.4,10.,EPS,IERR)
      IF(IERR) 1,2,1
    1 TE=.4
    2 CONTINUE
C RATE CONSTANTS - ELCTRONIC
      VD=SQRT(2*TE/MASM)*3E10
      J=NE*E*VD
      VDISC=V-R*J*A-L*A*E*VD*(NE-NEP)/DT
      NEP=NE
      RC=6.38E7*(SQRT(2*TE))**3
      R1=RC*EXP(-EM1/TE)*(1.+EM1/(2*TE))*(NE*CM1*M)
      R1B=(R1/M)*EXP(EM1/TE)*M1*.25
      R1X=RC*EXP(-EX1/TE)*(1.+EX1/(2*TE))*(NE*CX1*XE)
      R1XB=(R1X/XE)*EXP(EX1/TE)*XE1*.25
      R37=RC*EXP(-EM2/TE)*(1.+EM2/(2*TE))*(NE*CM2*M)
      R37B=(R37/M)*EXP(EM2/TE)*M2*.1
      R37X=RC*EXP(-EX2/TE)*(1.+EX2/(2*TE))*(NE*CX2*XE)
      R37XB=(R37X/XE)*EXP(EX2/TE)*XE2*.1
      R38=RC*EXP(-(EMI-EM1)/TE)*(1.+(EMI-EM1)/(2*TE))*
     +(NE*CM1I*M1)
      R39=RC*EXP(-(EMI-EM2)/TE)*(1.+(EMI-EM2)/(2*TE))*
     +(NE*CM2I*M2)
      R38X=RC*EXP(-(EXI-EX1)/TE)*(1.+(EXI-EX1)/(2*TE))
     ++*(NE*CX1I*XE1)
      R39X=RC*EXP(-(EXI-EX2)/TE)*(1.+(EXI-EX2)/(2*TE))
     ++*(NE*CX2I*XE2)
      R2=RC*EXP(-EMI/TE)*(1.+EMI/(2*TE))*(NE*CMI*M)
      R2X=RC*EXP(-EXI/TE)*(1.+EXI/(2*TE))*(NE*CXI*XE)
      R4=.29E-8*MDI*NE/(SQRT(TE))
      R4X=.346E-6*XEDI*NE/(SQRT(TE))
      R4MX=.346E-7*XEMI*NE/(SQRT(TE))
      R17 = 9.1E-10*TE**(-2.16)*EXP(-.165/TE)*NE*FL
      R28=2E-8*XEFU*NE
      R28B=2E-8*EXP(-EXEFU/TE)*NE*XEFG
      REL=(NE*CEL*M*SQRT(2*TE/MASE))*3E10*(2*MASE/MASM)*TE
```

```
C RATE CONSTANTS - GAS KINETIC
      SQRTG=SQRT(TG)
      K3X=1.E-23*EXP(.6/TG)
      K5X=1.E-23*EXP(1.5/TG)
      K41=1.E-23*EXP(.074/TG)
      G3=M*3.7E-31*M*MI*SQRTG
      G3X=XE*12E-31*M*XEI*SQRTG
      G3MX=M*5.8E-31*M*XEI*SQRTG
      G3XB=12E-31*XE*XEDI/K3X*SQRTG
      G5=M*12E-33*M*M1*SQRTG
      G5X=M*15E-32*XE*XE1*SQRTG
      G5MX=M*47E-33*M*XE1*SQRTG
      G5XB=15E-32*XE*XED1/K5X*SQRTG
      G13=29E-10*M1*XE*SQRTG
      G14=29E-10*MD1*XE*SQRTG
      G18=0; G18X=34.7E-10*SQRTG*XE1*FL
      G20=0; G20X=35E-10*XED1*FL*SQRTG
      G22=5E-7*MI*FNI*SQRTG
      G22X=17E-7*XEI*FNI*SQRTG
      G23=3E-25*MI*FNI*M*SQRTG
      G23X=12E-25*XEI*FNI*M*SQRTG
      G24=5E-7*MDI*FNI*SQRTG
      G24X=17E-7*XEDI*FNI*SQRTG
      G25=3E-25*MDI*FNI*M*SQRTG
      G25X=12E-25*XEDI*FNI*M*SQRTG
      G27X=46E-10*XEFU*FL*SQRTG
      G31=10E-10*M1**2*SQRTG
      G31X=30E-10*XE1**2*SQRTG
      G31MX=20E-10*XE1*M1*SQRTG
      G32=10E-10*M1*MD1*SQRTG
      G32X=30E-10*XE1*XED1*SQRTG
      G32MX=20E-10*M1*XED1*SQRTG
      G33=10E-10*MD1**2*SQRTG
      G33X=30E-10*XED1**2*SQRTG
      G33MX=20E-10*XEM1**2*SQRTG
      G34=10E-10*M1*XEFU*SQRTG
      G34X=30E-10*XE1*XEFU*SQRTG
      G34MX=0
      G35=10E-10*MD1*XEFU*SQRTG
      G35X=30E-10*XED1*XEFU*SQRTG
      G35MX=20E-10*XEM1*XEFU*SQRTG
      G40=F*1E-32*F*M*SQRTG
      G41=M*2E-32*XE*F*SQRTG
      G41B=2E-32*M*XEFG/K41
      G44=6E-32*F*XE1*M*SQRTG
      CSTIM=2.6E-17
C DIFFUSIN RATES
      KPLUS=.44E3*(3E16/(XE+M))*SQRT(.03/TG)
      KNI=2E3*(3E16/(XE+M))*SQRT(.03/TG)
      KEL=VD/(VDISC/LENGTH)
      DPLUS=12*(3E16/(XE+M))*SQRT(TG/.03)**3*(4.8/D)**2
```

```
      DNI=30*(3E16/(XE+M))*SQRT(TG/.03)**3*(4.8/D)**2
      DEL=SQRT(2*TE/MASE)*3E10/(3*CEL*(XE+M))*(4.8/D)**2
      DXE=SQRT(2*TG/MASXE)*3E10/(3*(M+XE)*CDIF)*(4.8/D)**2
      DM=DXE*SQRT(MASXE/MASM)
      DAPOS=DPLUS-KPLUS*(DPLUS*XEI-DNI*FNI-DEL*NE)/
     +(KPLUS*XEI+KNI*FNI+KEL*NE)
      DANEG=DNI+KNI*(DPLUS*XEI-DNI*FNI-DEL*NE)/(KPLUS*XEI+KNI*FNI+
     +KEL*NE)
C RATE EQUATIONS
      M1=M1+DT*(R1+R4+G22+G5B-G5-G18-R1B-G13-G31-DM*M1)
      M2=M2+DT*(R37+R4-AM2*M2-R37B)
      MI=MI+DT*(R2+G3B+R38+R39-G3-G22-G23-DAPOS*MI)
      XE1=XE1+DT*(R1X+R4X+G22X+G5XB-G5X-G18X-R1XB-G31X-R38X-DXE*XE1)
      XE2=XE2+DT*(R37X+R4X-AXE2*XE2-R37B)
      XEI=XEI+DT*(R2X+G3XB+G3MXB+G13+G14+R38X+R39X-G3X-G3MX-G22X-G23X
     +-DAPOS*XEI)
      MDI=MDI+DT*(G3+G31+G32+G33+G34+G35-R4-G24-G25-G35-DAPOS*MDI)
      XED1=XED1+DT*(G5X+G24X-AXED*XED1-G5XB)
      XEDI=XEDI+DT*(G3X+G31X+G32X+G33X+G34X+G35X-R4X-G24X-G25X-G3XB
     +-DAPOS*XEDI)
      XEM1=XEM1+DT*(G5MX+G24MX-AMX*XEM1-G5MXB)
      XEMI=XEMI+DT*(G3MX+G31MX+G32MX+G33MX+G34MX+G35MX-R4MX-G24MX-G25MX-
     +G3MXB-DAPOS*XEMI)
      FNI=FNI+DT*(R17-G22-G22X-G23-G23X-G24-G24X-G25-G25X-DANEG*FNI)
      FL=FL+DT*(R17B+G40-R17-G18-G18X-G20-G20X)
      XEFG=XEFG+DT*(AXEF*XEFU+R28+G27X+G35+G41+G35X-R28B-G41B)
      XEFU=XEFU+DT*(G18X+G20+G23X+G25X+R28B-AXEF*XEFU-G27X-R28-G34-G34X-
     +G35-G35X)
      F=F+DT*(R17+G18X+G20X+G22+G22X+G24+G24X+G25+G25X+2*G27X+G34+G34X+G
     +41B
     + -G44-G41-2*G40)
C GAS TEMPERATURE
      TG=TG+DT*2/(3*M)*(NE*VD*(VDISC/LENGTH)-(4.8/D)**2*K*(TG-TG0))
C GAIN
      GAIN=CSTIM*(XEFU-XEFG*EXP(-.074/TG))
C OUTPUT
      IF(ISTEP/IPRINT-FLOAT(ISTEP)/FLOAT(IPRINT)) 31,30,31
   30 CONTINUE
      WRITE(5,90) T,VDISC,J,NE,FNI,MI,XEI
   90 FORMAT(7(E10.2))
      WRITE(5, 95) FL,XE1,XEFU,XEFG,GAIN,TG,TE
   95 FORMAT(3X,7(E10.2))
   31 CONTINUE
      GO TO 20
   22 WRITE(5, 200)
  200 FORMAT(2X,19H>0, GO ON---<0, END)
      ACCEPT*,Z
      IF(Z ) 41,41,42
   42 WRITE(5, 250)
  250 FORMAT(2X,28HNEW VALUES: DT, TMAX, IPRINT)
      ACCEPT*,DT,TMAX,IPRINT
```

```
      ISTEP=0
      GO TO 20
      STOP
   41 END
      FUNCTION FUNC(TE)
      REAL M,M1,M2,NE,MASE,MASM,LENGTH,NEP,L
      COMMON/STOR/M,XE,NE,NEP,CM1,CX1,XEFG,EM1,EX1,EXEFU,CEL,
     +MASE,MASM,V,LENGTH,A,L,R,DT,E,FL
      VD=SQRT(2*TE/MASM)*3E10
      RC=6.38E7*(SQRT(2*TE))**3
      IF (TE-.4) 51,52,52
   51 R1=0.; R1X=0.; GO TO 53
   52 CONTINUE
      R1=RC*EXP(-EM1/TE)*(1.+EM1/(2*TE))*(CM1*M)
      R1X=RC*EXP(-EX1/TE)*(1.+EX1/(2*TE))*(CX1*XE)
   53 CONTINUE
      R17=9.1E-10*TE**(-2.16)*EXP(.165/TE)*FL
      R28B=2E-8*EXP(-EXEFU/TE)*XEFG
      REL=(CEL*M*SQRT(2*TE/MASE))*3E10*(2*MASE/MASM)*TE
      FUNC=(V-R*A*E*NE*VD-L*A*E*VD*(NE-NEP)/DT)/LENGTH
     + -(1/VD)*(R1X*EX1+R1*EM1+R17*TE+R28B*EXEFU+REL)
      RETURN;END
```

```
C KXECP - PULSED K-XE LASER
      REAL MASE,MASXE,MASH,M1,M2,MI,K,K3X,K5X,K41,NE0,NE
      REAL LAMDE,LAMDD,KAEX,KAD1,KXEX,KXDI
      REAL NEP
      REAL J
      REAL LENGTH
      REAL KPLUS,KNI,KEL
      REAL L
      EXTERNAL FUNC
      COMMON/STOR/XE,P0,CP1,CX1,NE,NEP,L,A,R,DT,E,
     + EP1,EX1,CEL,MASE,MASXE,V,LENGTH,P1,CP1I,CPI,EPI
      COMMON/STE/IE
C CONSTANT DATA
      MASE=0.5E6; E=1.6E-19; MASXE=131*1840*.5E6
      K=0
      C=2.7E-9
      D=1
      A=27
C XL=XENON
      LAMDE=.85E-4
      LAMDD=1.04E-4
      AP=3.69E7
      REX=3.7E-8
      RDI=5.4E-8
      RDIE=4.4E-8
      DRDFE=.53E-8/(579)
      DRDFD=1E-8/(.04E4)
      DRDFDE=.4E-8/(1.388E3)
      VEA=-.079
      VEX=.062
      VDA=-.66
      VDX=-.262
      VDXE=-.560
      EP1=1.61
      EP2=3.5
      EPI=4.34
      EPX1=1.46
      EPXI=4.19
      EPD1=1.46
      EPDI=4.19
      CP1=6E-15
      CP2=6E-16
      CPI=.5E-16
      CP1I=5E-16
      CPX1=6E-15
      CPXI=.5E-16
      CPD1=6E-15
```

```
      CPDI=.5E-16
      CPHI=.05E-18
      CEL=5.5E-16
      CDIF=1E-15
      SA=8.49E4;SB=7.18
      LENGTH=1
      K=160E19
      AX2=4E7;AP=3.69E7;AXED1=4E7
      CSTME=AP/2*LAMDE**2*REX**2*DRDFE
      CSTMD=AP/2*LAMDD**2*RDI**2*DRDFD
      CSTMDE=AP/2*LAMDE**2*RDIE**2*DRDFDE

C INITIAL CONDITIONS
      WRITE(5, 50)
   50 FORMAT(2X,2HXE,2X,2HTG,2X,1HW,2X,1HV,2X,1HC,2X,2HDT,2X,6HIPRINT,
     +2X,4HTMAX,2X,5HDELAY)
      ACCEPT*,XE,TG,W,V,C,DT,IPRINT,TMAX,DELAY
      P0=2.7E16*(273/(273+TG))*10**(SB-.052*SA/(TG+273))
      TG=(TG+273)*(1/1.16E4)
      TG0=TG
      F=W/(1.6E-19*EPI)*(1.24/EPI-.2)
       KXDI=1.8E-22*EXP(.56/TG)
      KXEX=2.2E-23*EXP(-.05/TG)
      PX=KXEX*P0*XE
      PD=KXDI*P0**2
      PX=KXEX*P0*XE
      PI=F*CPHI*P0*DELAY
      P1=10.*PI
      AT=AP*1.6/(8.3E-15*P0*D)
      IF(AT-AP)18,17,17
   17 AT=AP
   18 CONTINUE
      WRITE(5, 82) P0,PD,PI
   82 FORMAT(2X,'P0=',E10.3,5X,'PD=',E10.3,5X,'PI=',E10.3)
      WRITE(5, 80)
   80 FORMAT(4X,4HTIME,6X,5HVDISC,5X,1HJ,9X,2HNE,8X,2HPI,
     +8X,3HPX1,7X,3HPD1)
      WRITE(5, 85)
   85 FORMAT(7X,1HP,9X,2HP1,8X,5HGAINE,5X,5HGAIND,5X,5HBETAE,5X,5HBETAD,
     +5X,2HTE)
C TIME STEP
   20 ISTEP=ISTEP+1
      T=T+DT
      IF(T-TMAX) 21,21,22
   21 CONTINUE
C CIRCUIT RESPONSE
      P=P0-(P1+PI)
      NE=PI
      V=V-DT*J*A/C
      IERR=0;IND=1;EPS=0.01
      TE=SOLN(IND,FUNC,.1,5.,EPS,IERR)
```

```
      IF(IERR) 1,2,1
    1 WRITE(5,*) IERR;GO TO 30
      STOP
    2 CONTINUE
C RATE CONSTANTS - ELCTRONIC
      VD=SQRT(2*TE/MASXE)*3E10
      J=NE*E*VD
      VDISC=V-R*J*A-L*A*E*VD*(NE-NEP)/DT
      NEP=NE
      RC=6.38E7*(SQRT(2*TE))**3
      RP1=RC*EXP(-EP1/TE)*(1+EP1/(2*TE))*(NE*CP1)*P
      RP1B=RP1/P*EXP(EP1/TE)*P1*.33
      RPI=RFN(EPI)*(NE*CPI)*P
      RP1I=RFN(EPI-EP1)*(NE*CP1I)*P1
      RPX1=RFN(EPX1)*(NE*CPX1)*PX
      RPX1B=RPX1/PX*EXP(EPX1/TE)*PX1*.5
      RPXI=RFN(EPXI)*(NE*CPX1)*PX
      RPD1=RFN(EPD1)*(NE*CPD1)*PD
      RPD1B=RPD1/PD*EXP(EPD1/TE)*PD1*1.
      RPDI=RFN(EPDI)*(NE*CPDI)*PD
      RECP=PI*2.28E-26*NE*TE**(-4.39)*NE
      RECPX=3.3E-5*TE**(-.67)*PXI*NE
      RECPD=3.3E-5*TE**(-.67)*PDI*NE
C RATE CONSTANTS - GAS KINETIC
      SQRTG=SQRT(TG)
      KAEX=2.2E-23*EXP(.074/TG)
      KADI=6.5E-23*EXP(.735/TG)
      KXEX=2.2E-23*EXP(-.05/TG)
      KXDI=1.8E-22*EXP(.56/TG)
      GPX=XE*8E-32*XE*P1
      GPXB=XE*8E-32/KAEX
      GPD=P*(XE*8E-30*P1)
      GPDB=(XE*8E-30)/KADI
      GPXI=(XE*8E-32*XE)*PI
      GPX1B=(XE*8E-32*PXI)/KAEX
      GPDI=(XE*8E-30*P)*PI
      GPDIB=(XE*8E-30*PDI)/KADI
C DIFFUSION RATES
      KPLUS=2E3*(3E16/(XE))*SQRT(.03/TG)
      KBL=VD/(VDISC/LENGTH)
      DXE=SQRT(2*TG/MASXE)*3E10/(3*(XE)*CDIF)*(4.8/D)**2
      DAPOS=KPLUS*TE*(4.8/D)**2
      DP=DXE*1.8
C RATE EQUATIONS
      P1=P1+DT*(RP1+RECP+RECPX+RECPD-RP1B-AP*(PX1+PD1)-DP*P1)
      IF (P1/P-3*EXP(-EP1/TE)) 8,9,9
    9 P1=P*3*EXP(-EP1/TE)
    8 CONTINUE
      PX=KXEX*P*XE
      PD=KXDI*P**2
      PI=PI+DT*(RPI+RP1I+RP2I+GPN*P+P*CPHI*F-RECP-RECPX-RECPD-DAPOS*PI)
```

```
        PX1=GPX/(GPXB+AP)
        PXI=KAEX*PI*XE
        PD1=GPD/(GPDB+AP)
        PDI=KADI*P*PI
  C GAS TEMPERATURE
        TG=TG+DT*(NE*VD*VDISC/LENGTH-(4.8/D)**2*K*(TG-TG0))*2/(3*XE)
  C GAIN
        BETAE=CSTME*2*P*XE*EXP(-VEX/TG)/3E10+CSTMDE*P**2*EXP(-VDXE/
       +TG)*.25/3E10
        BETAD=CSTMD*P**2*EXP(-VDX/TG)*.25/3E10
        GAINE=CSTME*(PX1*EXP(-VEA/TG)/(KAEX*1.5)-2*P*XE*EXP(-VEX/TG))/3E10
       +-CSTMDE*(P**2*EXP(-VDXE/TG)*.25)/3E10
        GAIND=CSTMD*(PD1*EXP(-VDA/TG)/(KADI*12)-P**2*EXP(-VDX/TG)*.25)
       +/3E10
  C-OUTPUT
        IF(ISTEP/IPRINT-FLOAT(ISTEP)/FLOAT(IPRINT)) 31,30,31
     30 CONTINUE
        WRITE(5,*) TG
        WRITE(5,90) T,VDISC,J,NE,PI,PX1,PD1
     90 FORMAT(7(E10.2))
        WRITE(5, 95) P,P1,GAINE,GAIND,BETAE,BETAD,TE
     95 FORMAT(3X,7(E10.2))
     31 CONTINUE
        GO TO 20
     22 WRITE(5, 200)
    200 FORMAT(2X,19H>0, GO ON---<0, END)
        ACCEPT*,Z
        IF(Z ) 41,41,42
     42 WRITE(5, 250)
    250 FORMAT(2X,28HNEW VALUES: DT, TMAX, IPRINT)
        ACCEPT*,DT,TMAX,IPRINT
        ISTEP=0
        GO TO 20
        STOP
     41 END
        FUNCTION FUNC(TE)
        REAL NE,MASE,MASXE,LENGTH,NEP,L
        COMMON/STOR/XE,P0,CP1,CX1,NE,NEP,L,A,R,DT,E,
       + EP1,EX1,CEL,MASE,MASXE,V,LENGTH,P1,CP1I,CPI,EPI
        VD=SQRT(2*TE/MASXE)*3E10
        RC=6.38E7*(SQRT(2*TE))**3
        RP1=RC*EXP(-EP1/TE)*(1+EP1/(2*TE))*CP1*P0
        REL=(CEL*XE*SQRT(2*TE/MASE))*3E10*(2*MASE/MASXE)*TE
        FUNC=(V-R*A*E*NE*VD-L*A*E*VD*(NE-NEP)/DT)/LENGTH
       + -(1/VD)*(RP1*EP1+REL)
        RETURN;END
        FUNCTION RFN(Y)
        COMMON/STE/TE
        RFN=6.38E7*(SQRT(2*TE))**3*EXP(-Y/TE)*(1+Y/(2*TE))
        RETURN;END
*

 EX$

OUTPUT FILE: KXETV.FOR;15 [New version]
@
```